CHALMERS
UNIVERSITY OF TECHNOLOGY

Investigation of the heat efficiency of a primary reformer at an ammonia plant in Indonesia

Master of science thesis

PONTUS NORELL

Department of Chemistry and Chemical Engineering
CHALMERS UNIVERSITY OF TECHNOLOGY
Gothenburg, Sweden 2015

Investigation of the heat efficiency of a primary reformer at an ammonia plant in Indonesia

PONTUS NORELL

Department of Chemistry and Chemical Engineering

Chalmers University of Technology

SE-412 96 Gothenburg

Sweden

Telephone + 46 (0)31-772 1000

Cover:

Photo of the interior of the primary reformer furnace

Picture taken by Pontus Norell

Gothenburg, Sweden 2015

Investigation of the heat efficiency of a primary reformer at an ammonia plant in Indonesia

PONTUS NORELL

Examiner:

Associate professor Ronnie Andersson, Chemical Engineering, Chalmers University of Technology

Supervisor:

Ph.D. Muslikhin Hidayat, Gadjah Madah University

Department of Chemistry and Chemical Engineering
CHALMERS UNIVERSITY OF TECHNOLOGY
Gothenburg, Sweden 2015

Investigation of the heat efficiency of a primary reformer at an ammonia plant in Indonesia

PONTUS NORELL
Department of Chemistry and Chemical Engineering
Chalmers University of Technology

Abstract

The nitrogen fertilizer urea, produced from ammonia, is important for Indonesian agriculture. At the ammonia plant large amount of hydrogen is required. It is produced by steam reforming of natural gas in the primary reformer consisting of a large furnace with hundreds of reactor tubes. The highly endothermic reforming reactions inside the tubes are heated by combustion of mainly natural gas in 200 burners located in the ceiling of the furnace.

This project was executed at a university in Indonesia in collaboration with a large urea producer. The objective was to investigate the reasons behind the higher fuel consumption of natural gas for the actual conditions of the plant compared to the design data.

An energy balance over the furnace was performed and it was identified that the actual data had higher losses and higher amount of recovered heat in the convective section. Furthermore, calculations of adiabatic flame temperature and energy demand, for various fuel compositions were performed.

The mixing of fuel and air in the burner and furnace was simulated by computational fluid dynamics and the simulations with design and actual data were compared. A more efficient mixing was observed for the actual data, which resulted in a slightly higher temperature in the upper part of the furnace. The uncertainties behind these results are discussed along with other explanations to the increased fuel consumption.

Keywords: Primary reformer, steam methane reforming, combustion, computational fluid dynamics

Preface

This master thesis is the result of a three month stay in the city of Yogyakarta in Indonesia. The project was made possible through the collaboration between Chalmers University of Technology in Gothenburg city and Gadjah Mada university (UGM) of Yogyakarta. Students from the two universities have the possibility to work abroad thanks to the Linnaeus-Palme exchange program. The results are increased knowledge, new perspectives and increased cultural awareness for both parts through the exchange of ideas and experiences.

The project is related to the heat efficiency of a process unit at a production plant for ammonia, situated in Indonesia. The ammonia is used for the synthesis of the fertilizer urea. Improving the heat efficiency is an important objective for several reasons. The most important are to reduce fossil fuel consumption, CO_2 emissions and operation cost for the production plant. It could also indirectly lead to an aid in the food supply to the Indonesian population, through cheaper fertilizers.

In the following technical report, I have tried to analyze and discuss the problem from various angles from an overall perspective and also by a more detailed investigation of the combustion process. I hope that my work will provide a deeper understanding of the problem and that it will help in the continuing efforts to reduce the fuel consumption of the primary reformer.

Acknowledgments

I would like to thank the following persons for making this thesis possible:

-Associate professor Ronnie Andersson for supervision and consultation
-Ph.D Muslikhin Hiyadat for supervision and consultation
-Professor Bengt Andersson for consultation
-Professor Claes Niklasson for helping me with travel arrangements
-The company contact person (who decided to be anonymous) for consultation and providing data

I am grateful to SIDA, Universitas Gadja Mada (especially the department of chemical engineering) and the fertilizer company (who decided to be anonymous) for giving me the opportunity of doing this project.

Finally, a special thanks to all my new friends in Yogyakarta, who took care of me and made me feel welcome during my three month stay in Indonesia!

Table of contents

1 Introduction 1

1.1 Agriculture and fertilizers 1

1.2 Indonesia and fertilizers 1

1.3 Natural gas and fertilizer production 1

1.4 Problem formulation 2

1.5 Project aim 2

1.6 Limitations 2

1.7 Objective 2

2 Theory 4

2.1 Urea 4

2.2 The Haber-Bosch process of ammonia synthesis 4

2.3 Production of hydrogen 4

2.4 Natural gas-based ammonia synthesis 5

2.5 Reforming reactions in the primary reformer 7

2.6 Heat transfer in the primary reformer 7

2.7 Burner arrangement in the primary reformer 8

2.8 Catalyst 8

2.9 Computational fluid dynamics 9

2.9.1 General procedure 9

2.9.2 Mesh 10

2.10 Governing equations 10

2.10.1 The equation of continuity 10

2.10.2 The Navier-Stokes equations 10

2.11 Turbulence 11

2.11.1 Reynolds decomposition 11

2.11.2 The Boussinesq approximation 12

2.11.3 Two equation models 12

2.11.4 The standard k- ε model 12

2.11.5 The realizable k- ε model 13

2.12 Reactions and mixing 13

2.12.1 Mixture fraction 14

2.12.2 β-PDF 15

2.12.3 Look up table 16
3 Method 17
3.1 Data gathering & mass balance calculations 17
3.2 Energy balance and adiabatic flame temperature 17
3.3 CFD 17
3.3.1 Geometry 17
3.3.2 Mesh 19
3.3.3 Models 20
3.3.4 Setup 21
4 Results and analysis 23
4.1 Energy balance 23
4.2 Adiabatic flame temperature 23
4.3 CFD simulations 25
4.3.1 Grid independence 25
4.3.2 Effect of turbulence 26
4.3.3 Design vs actual 28
5 Discussion 32
6 Conclusions 34
7 Further investigations 35
References 36
Appendix A – The fuel streams and their compositions ..... A
Appendix B – Inlet compositions for actual and design simulations ..... B
Appendix C – Calculation of fuel consumption C

1 Introduction

In this project an ammonia plant in Indonesia is investigated. The ammonia is used to produce urea which is a nitrogen fertilizer. The investigation regards the energy efficiency in respect to natural gas consumption of the process unit known as the primary reformer for production of synthesis gas.

1.1 Agriculture and fertilizers

Nitrogen is a very important element for plants since it is one of the building blocks for many vital parts of the cell such as amino acids, nucleic acids and chlorophyll. Although the atmosphere constitutes large quantities of nitrogen gas (N_2) and living organisms only need small amounts of nitrogen, it is usually the limiting factor for growth [1]. This is due to the high stability of the nitrogen gas which inhibits most plants from absorbing nitrogen directly from the air. The strong bond between the two nitrogen atoms has to be broken first. This can naturally happen in two ways: by lightning and by nitrogen fixating bacteria (the most important living on roots of legumes).

When humans started producing fixed nitrogen in the form of ammonia (NH_3), that could be used to produce nitrogen fertilizers the modern agriculture was changed in a revolutionary way. Today the world food production is highly dependent on this process and in the mid 1990s it provided food to the survival for 40% of the world population [1]. Due to the expected increase of population in the low income countries, the desire to provide more nutritious food (especially in respect to protein) and the need to eliminate malnutrition and stunting it is necessary to further increase the production of ammonia.

The anthropogenic addition of fixed nitrogen has significantly disturbed the natural flows of the element [1]. The most important concern is leaching of nitrogen from the fields to different waters, which can lead to eutrophication and poisoning of drinking water. Losses of nitrogen to the atmosphere in the form of different nitrogen oxides is another concern which contributes to global warming and destruction of the ozone layer. To reduce these factors a better handling of both synthetic fertilizers and manures should be applied, to reduce the losses. Important measures to reduce the overall consumption of nitrogen fertilizers includes more usage of leguminous crops in the fields, reducing food wastes and switching to a more healthy diet based on lower meat consumption in the high income countries.

1.2 Indonesia and fertilizers

Indonesia is the fourth most populous country in the world. Securing food supply to the population is an important objective for the Indonesian government [2]. Significant improvements have been achieved in the last decade but $8.7\ \%$ of the population remain undernourished. The main strategy from the Indonesian government has been to apply several subsidies (around USD 2 billion was spent in 2014), including cheaper fertilizers to small scale domestic farmers. Almost $40\ \%$ of the labor force work in the agricultural sector and it is very important to increase the agricultural productivity and efficiency to counteract poverty and further develop the economy of the country [3].

1.3 Natural gas and fertilizer production

Fertilizer production belongs to the key energy intensive industries of the world with $1.2\ \%$ of the energy consumption, where over $90\ \%$ of this energy is consumed in the ammonia production [4]. Newer production plants are however much more energy efficient than older plants and the same is true for natural gas based plants compared to coal based.

In Indonesia the natural gas accounts for $50 - 60$ % of the total production cost of urea [5]. This, as well as reducing CO_2 emissions, makes it of high importance to run the production plants as energy efficient as possible, especially since the subsidy on natural gas for Indonesian fertilizer companies was removed in 2001.

1.4 Problem formulation

The primary reformer is the production unit for synthesis gas from natural gas and steam. The overall reaction is highly endothermic and requires supply of heat. Therefore, the reaction takes place inside tubes placed in a furnace. The heat is produced by combustion in burners placed in the furnace.

The Indonesian company for which this project was performed is an important urea producer. The primary reformer at one of their ammonia plants consists of an approximately 10 m high furnace, referred to as the "radiant section". In the radiant section there are 378 tubes to which heat is supplied from 200 burners located in the ceiling. After heating process gas inside the tubes, the flue gases leave the radiant section and enter the "convective section", where heat is recovered to different streams of the plant before leaving to the atmosphere.

The company has found by doing energy balance calculations that their primary reformer consumes more energy (for combustion) than it was designed for. The fuel consists primarily of natural gas but since a few years ago a big amount of recycled tail gas from the Purge gas recovery unit has been added. There is also a smaller amount of heavy hydro carbon gas added to the fuel. (See Appendix A for the fuel streams and their compositions).

Since the actual data shows a higher energy consumption than the design data, engineers at the company think that it should be possible to reduce the consumption of natural gas as fuel.

1.5 Project aim

The aim of this project was to obtain better understanding of the reason behind the higher fuel consumption in the actual data compared to the design data; and try to find possible improvements.

1.6 Limitations

The ammonia plant has a complex infrastructure with many parts that affect each other. There can be several reasons behind the increased fuel consumption and several possible improvements as well. This project had to be limited in some way to make sense. For this reason, the focus was on comparing the design data with the actual data to hopefully identify differences that could explain why the fuel consumption had increased. Due to the great number of possible comparisons one could do, the number of parameters to analyze also had to be limited. Therefore, the following things were chosen for the investigation: Mass and heat balances over the radiant section, how the composition affects the adiabatic flame temperature and if there could be a problem with the mixing of the fuel and the air.

1.7 Objective

Based on the project aim and the limitations the objective could be specified in detail as a couple of questions which are listed here.

- What are the possible improvements based on overall supply and demand of energy in the primary reformer?
- How does the composition of the fuel affect the adiabatic flame temperature?

- Could it be possible to change the fuel composition to reduce the amount of natural gas?
- Are there any differences in the combustion process with respect to the mixing of fuel and air that could explain the higher fuel consumption?

2 Theory

2.1 Urea

Urea is the most important nitrogen fertilizer in the world with 56% of the market 2010 [6]. Some reasons for this include its high nitrogen content (46%) and that it is easy to use in the fields [1]. It is a solid fertilizer with the chemical formula $CO(NH_2)_2$.

Urea is made from liquid ammonia and carbon dioxide and the process takes place under high temperature and pressure, requiring a lot of energy [1]. The steps are first the production of ammonium carbamate and then removal of water to obtain the solid form of urea.

$$2NH_3 + CO_2 \rightarrow NH_2CO_2NH_4 \quad (1)$$

$$NH_2CO_2NH_4 \rightarrow CO(NH_2)_2 + H_2O \quad (2)$$

When dissolved in water urea is slowly converted to ammonia and carbon dioxide; this is the reason why urea is useful as a nitrogen fertilizer. The ammonia is then converted by natural microbial processes to nitrogen compounds that the crops can take up and use in their growth [1].

2.2 The Haber-Bosch process of ammonia synthesis

The large scale production of ammonia started in the early 1900s [1]. The process is named after Fritz Haber and Carl Bosch, the former showed that it was possible to synthesize ammonia from its elements (H_2 and N_2) and the latter was the main character who lead way to its commercialization. There were of course several other important contributors involved in the development as well. The most important factors for the success were high pressure, finding the optimal catalyst, recirculation of unreacted reactants, providing cheap and clean raw material and making sure the equipment would endure the severe process conditions. The reaction is, despite of this, quite simple and exothermic.

$$N_2 + 3H_2 \leftrightarrow 2NH_3 \quad (3)$$

This project is related to the production of one of the two reactants, namely hydrogen. Meanwhile nitrogen easily can be accessed from the abundant storage in the atmosphere, the hydrogen is more complicated to obtain. In fact, it is the production of hydrogen that is, -and always has been-, the most expensive part in the entire ammonia synthesis process.

2.3 Production of hydrogen

Hydrogen gas can be produced from hydrocarbons, water and biomass. The ammonia industry consumes 54 % of the produced hydrogen. Natural gas is the major source industrially, but light alcohols is also of importance. The industrial methods can be classified in four categories [7]:

i) Steam methane reformation (SMR):
Uses light gaseous or liquid hydro carbons in combination with steam. The endothermic reaction

takes place in catalyst filled tubes with an external heat source. $40 - 50\ \%$ of the hydrogen is produced by this method.

ii) Partial oxidation (POX):
Hydro carbons are heated together with a limited amount of pure oxygen. It is expensive due to the requirement of pure oxygen.

iii) Auto-thermal reformation (ATR):
Natural gas is partly combusted with oxidizer (air or oxygen) to provide heat and partly catalytically reformed with steam.

iv) Steam-iron process:
Involves a two-step redox reaction. Coal, oil or biomass is used to produce a gas which reduces an iron oxide. Then steam is reduced to hydrogen gas together with re-oxidation of the iron oxide to its initial state.

The hydrogen production in the ammonia plant uses a serial configuration with SMR and ATR, known as the primary reformer and the secondary reformer, respectively. The primary reformer is known for high capacity and the secondary reformer is known for lower fuel consumption and lower CO_2 emissions. By combining them a desirable balance between these targets can be achieved [8].

There is a high interest in the production of hydrogen from renewable and sustainable sources [7]. A lot of research is going on. Some promising technologies are plasma reforming, thermochemical splitting of water and a few biological processes.

2.4 Natural gas-based ammonia synthesis

During the evolution of the ammonia synthesis, industrial plants have used feed-stocks originating from coal, crude oil, lignite and natural gas [1]. Of these, natural gas is the most efficient since gases are easier to handle in continuous processes and because methane (CH_4), the main constituent of natural gas, has the highest $H:C$ ratio of all hydrocarbons. For the production of urea, the smaller amounts of other light alkanes in natural gas is beneficial for the carbon dioxide needed downstream in the process. Today the large majority of ammonia plants run on natural gas, both as raw material and fuel.

The general steps in the synthesis of ammonia in natural gas-based plants is presented in Figure 1 [1].

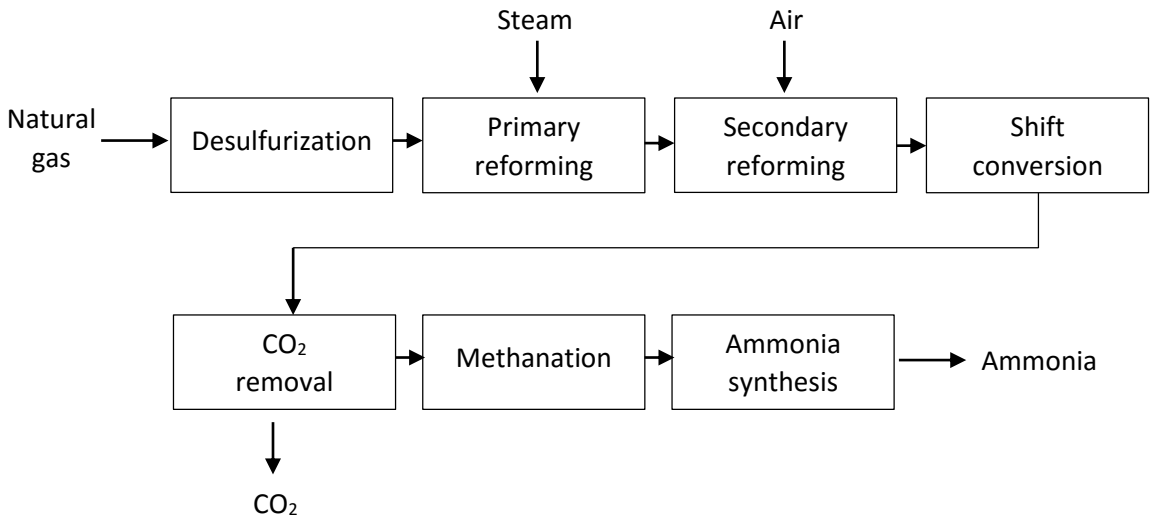

Figure 1. General process steps in natural gas-based ammonia synthesis.

Firstly, the natural gas is cleaned from sulfur to avoid poisoning of the catalyst.

Then it is mixed with steam and enters the primary reformer, in which the majority of the natural gas is converted to synthesis gas through the highly endothermic reforming reactions.

In the secondary reformer unreacted methane from the primary reformer is partly combusted to provide heat and partly reformed further. The combustion air is added to achieve the needed amount of nitrogen for the ammonia synthesis.

In the shift converter more hydrogen is produced through the slightly exothermic shift reaction.

CO_2 is removed through an absorption process. If the plant is in connection with a urea plant this CO_2 is used in the urea production.

To avoid poisoning of the catalyst in the ammonia synthesis the minor amounts of CO and CO_2 that still remains in the gas mixture are converted through the reversed reforming- and shift reactions in the methanator.

Finally, water is removed and the gas containing the stoichiometric amount of N_2 to H_2 is converted under high pressure to ammonia through the ammonia synthesis reaction, Eq. (3), The final product is liquid ammonia.

2.5 Reforming reactions in the primary reformer

The reactions for synthesis gas production taking place inside the reformer tubes are presented below [9,10]. All of them are reversible except reaction (5), i.e. higher hydrocarbons than methane have $100\ \%$ conversion to carbon monoxide and hydrogen under normal reforming conditions.

$$CH_4 + H_2O \leftrightarrow CO + 3H_2 \tag{4}$$

$$C_nH_m + nH_2O \rightarrow nCO + (n + 0.5m)H_2 \tag{5}$$

$$CO + H_2O \leftrightarrow CO_2 + H_2 \tag{6}$$

$$CH_4 + 2H_2O \leftrightarrow CO_2 + 4H_2 \tag{7}$$

It can be seen, from Le Chatelier's principle, that a high steam to carbon ratio at the inlet will favor hydrogen production for all the reactions (4-7), high temperature will move the equilibrium towards the right for the endothermic reactions (4), (5) and (7) and a low pressure will have a positive effect on the equilibrium condition for all of the reactions except reaction (6) which is unaffected. Based on these equilibrium considerations the primary reformer in this investigation uses a steam to carbon ratio for the feed at the top of the tubes of approximately 3. The process gas is then heated to a high temperature around $800\ ℃$. In contradiction to optimal equilibrium conditions the pressure inside the tubes are high, above $30\ bar$, this has to do with practical considerations such as reducing equipment size and that downstream process units require the process gas at an elevated pressure. There is no doubt that the right equilibrium conditions at the tube outlet is critical for the reformation, but reaction kinetics and diffusional limitations are also of importance [10,11].

2.6 Heat transfer in the primary reformer

The transfer of heat from the flames to the tubes occurs directly, mainly by radiation but also by convection, and indirectly from the hot walls of the furnace with radiation. To maintain stable conditions the heat transfer from the flames to the process gas must be equal to the rate at which it is absorbed by the reforming reaction and the rate by which it is transported by the flow in the tubes. Even a small increase in tube wall temperature might lead to serious shortening of the expected tube life time.

Typically, $50\ \%$ of the heat is transferred to the tubes ($60\ \%$ used for reaction and $40\ \%$ used for raising the temperature). The rest is recovered in the convective section, which can lead to heat efficiencies reaching $95\ \%$ [9].

Several simulations where models for the reformation in the tubes in combination with the heat transfer from the furnace have been performed [11-17]. Some findings for increased heat transfer and thereby higher reformation efficiency are listed here:

- Higher emissivity for the furnace and tube walls increases radiative heat transfer to the tubes
- Lower absorption coefficient of radiation for the combustion gases increases radiative heat transfer to the tubes
- Convective heat transfer rate can be increased with higher furnace pressure
- Recirculation of combustion gases at the furnace inlet can give rise to increased heat transfer due to faster combustion
- Lower tube pitch ratio gives a more efficient radiation heat transfer

2.7 Burner arrangement in the primary reformer

There are basically four types of reformer furnaces regarding burner arrangement: bottom fired, terrace wall, top fired and side fired [9]. These are illustrated in Figure 2. The position of the burners strongly affects the temperature profile of the tube wall and the heat flux profile along the tubes. The bottom fired arrangement is characterized by a constant heat flux profile, independent of vertical location, which results in high temperatures of the tube wall close to the bottom. This effect can be mitigated with the terrace wall design. In a top fired furnace the heat flux is much larger in the upper part of the furnace while the tube wall temperature is close to constant with a maximum in the upper part. The side fired furnace has several advantages compared to the top fired. It shows more even heat flux and tube wall temperature which makes it possible to transfer more heat with less stress on the tubes.

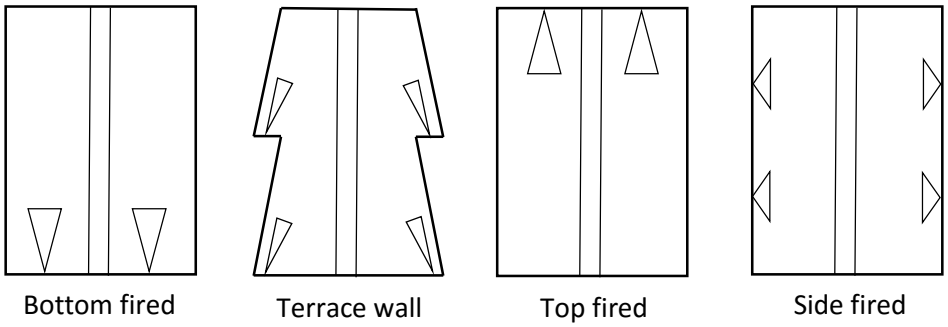

Figure 2. Burner arrangements in the reformer furnace.

2.8 Catalyst

The catalyst used for steam reforming in industrial processes is for most cases nickel. Other more active metals exist, but nickel has been the most economical option. Deactivation of the catalyst is a concern and the company do have to replace it every 5 years or so. The capacity can, however, be maintained if the loss of activity is compensated for by a higher heat transfer rate, but this results in an increase of the tube wall temperature [9]. A margin accounting for this effect is therefore necessary to avoid damaging the tube material.

The causes for deactivation relevant for industrial steam reforming are sulfur poisoning, sintering [18] and coking [19,20]. Sulfur poisoning should not be of any concern since it is removed from the natural gas in the desulfurizer prior to the primary reformer, see Figure 1.

Sintering is the diffusive process when nickel particles are merged together with the outcome of reduced active area. High temperature and steam pressure increase the sintering rate while larger surface area of the carrier reduces the effect.

Formation of coke by the reactions (8-11) at the active site of the nickel catalyst has to be considered especially because of the high temperatures in the reactor.

$$2CO \leftrightarrow C + CO_2 \tag{8}$$

$$CH_4 \leftrightarrow C + 2H_2 \tag{9}$$

$$CO + H_2 \leftrightarrow C + H_2O \tag{10}$$

$$C_nH_m \rightarrow nC + 0.5mH_2 \tag{11}$$

The carbon deactivates the catalyst either by blocking the active site or by blocking the pore openings of the support. Another problem with coke formation is that it may eventually cause a damaging increase of the pressure drop in the reactor. It is probable that the undesired carbon forming reactions take place simultaneously with the desired steam reforming reactions Eq. (4-7) through a joint intermediate. Despite of this, several measures can minimize coking. One is to use a high steam to carbon ratio and thereby increase the rate of gasification of the deposited carbon through the reverse of reaction (10).

2.9 Computational fluid dynamics

Computational fluid dynamics (CFD) is a method to solve the non-linear mass-, momentum- and energy balance equations describing a system consisting of flowing fluids. Based on the computational power available, some phenomena, such as turbulence, heat transfer and chemical reactions, might have to be simplified to some extent with different models.

Performing design improvements on a full size primary reformer comes with a great cost. Therefore, several approaches to model it have been performed [12,13] and [15-17]. CFD is a promising tool that can be used to analyze reforming performance. One successful study is [21] in which a new reactor design was compared with an older design.

When using CFD one has to be careful when interpreting the results. The calculated solution can be dependent on the mesh and the chosen models. To be able to understand how reliable the solution is one has to have sufficient knowledge about the numerics behind the solution as well as about the limitations of the models used.

2.9.1 General procedure

There exist several CFD programs adapted for a wide range of applications. The procedure is often similar. First the geometry of the system is drawn in a CAD program. The geometry can be either 2D or 3D. Then the mesh is created. It consists of control volumes over which the equations are discretized based on averaging. After this any models needed for the particular system have to be chosen and possibly adjusted by changing certain parameters. Physical properties of the fluid and boundary conditions is specified as

well. The algorithm for the solver and some solver settings have to be set. An initial guess for the values of all the variables is required for steady-state calulations before the simulation can start. When a converged solution is reached the accuracy and reliability of the results have to be evaluated in different ways [22].

2.9.2 Mesh

The approximation of the equations introduces numerical errors in the solution. The smaller the cells become the more reduced are the numerical errors. Unfortunately, smaller cells mean more cells and the computational cost is increased. Hence, there has to be a balanced choice between sufficient accuracy and reasonable simulation time.

The features of the mesh have a big impact on the convergence and accuracy of the solution. Preferably the mesh should consist of hexahedral elements which requires less memory and enables better convergence than meshes involving tetrahedral elements and other element shapes. For complex geometries it can unfortunately be impossible to only use hexahedral elements. The cells at boundaries, especially walls, should be aligned with the boundary (close to $90°$ angle) and it is advantageous to have all cells aligned with the flow (of course only possible for hexahedral cells). A mesh with cells of similar sizes generally gives more accurate solution, but to balance computational time with accuracy, denser mesh can be used in regions with large gradients while coarser mesh can be applied where the calculated variables are not changing as much. An example of a region with large gradients is close to walls where the velocity changes rapidly from its mean flow rate to zero at the wall.

The quality of the cell elements is also important for convergence and accurate results [22]. The skewness is a measure of how equiangular or equilateral the cell elements are. It is recommended to have the average skewness below 0.33 and the maximum skewness below 0.95. The aspect ratio is a measure on how stretched the cell elements are. Optimally the aspect ratio should be one for all elements, but can be up to 5 in a direction where gradients of the variables are small. At and along the walls aspect ratios up to 20 could work since the flow is aligned with the wall. Another useful quality measure is the orthogonal quality. This measure includes the symmetry of the individual cells as well as their symmetry with adjacent cells. Orthogonal quality lies between zero and one, where low values are bad and high values are good. A good orthogonal quality is especially important at the boundaries.

2.10 Governing equations

In this chapter the governing equations solved in CFD are presented [22].

2.10.1 The equation of continuity

The equation of continuity is based on a mass balance over a fluid volume. For the assumption of incompressible flow, the continuity equation is:

$$\frac{\partial U_i}{\partial x_i} = 0 \tag{12}$$

Where U is the velocity.

2.10.2 The Navier-Stokes equations

The Navier-Stokes equations are obtained by setting the change of momentum for a fluid volume equal to the forces acting on it. For a 3D simulation there will be three equations, one for each direction. Assuming Newtonian fluid, incompressible flow and macroscopic conditions for the flow, the equations are:

$$\frac{\partial U_i}{\partial t} + U_j \frac{\partial U_i}{\partial x_j} = -\frac{1}{\rho}\frac{\partial P}{\partial x_i} + \upsilon \frac{\partial^2 U_i}{\partial {x_j}^2} \tag{13}$$

Where P is the pressure, ρ is the density of the fluid and υ is the kinematic viscosity of the fluid.

2.11 Turbulence

Turbulence is a property of the flow and is characterized by chaotic and irregular patterns [23]. It arises when the inertial forces of the flow overcome the dampening viscous forces of the fluid. This can be quantified by the Reynolds number.

$$Re = \frac{L\langle U \rangle}{v} \tag{14}$$

Where $\langle U \rangle$ is the average velocity, L is a characteristic length of the system and v is the kinematic viscosity.

The transition to turbulent flow occurs at a high enough Reynolds number. This value is different for different systems. Turbulence is also a decaying process, meaning that energy has to continuously be added to sustain it. Two desirable properties of turbulent flow are that it increases the heat- and mass transfer significantly compared with laminar flow. An undesired effect on the other hand is the increased pressure drop due to increased friction with walls.

Turbulent flows are complex and very computationally expensive to solve completely. Therefore, the smaller turbulent scales in the turbulence transport equation are simplified by other relations. These relations usually include unknown variables that need to be determined and this is what the different turbulence models do. In this section the basis for the two turbulence models used in this project, the standard and the realizable k-ε model, are described.

2.11.1 Reynolds decomposition

The basis for the turbulence models used in engineering simulations is the Reynolds decomposition where the instantaneous velocity and pressure is separated in a mean part and a fluctuating part.

$$U_i = \langle U_i \rangle + u_i \tag{15}$$

$$P = \langle P \rangle + p \tag{16}$$

Eq. (15) and (16) are inserted into the continuity equation, Eq. (12), and into the Navier-Stokes equations, Eq. (13), which gives the following equations:

$$\frac{\partial \langle U_i \rangle}{\partial x_i} = 0 \tag{17}$$

$$\frac{\partial \langle U_i \rangle}{\partial t} + \langle U_j \rangle \frac{\partial \langle U_i \rangle}{\partial x_j} = -\frac{1}{\rho}\frac{\partial}{\partial x_j}\left\{\langle P \rangle \delta_{ij} + \mu\left(\frac{\partial \langle U_i \rangle}{\partial x_j} + \frac{\partial \langle U_j \rangle}{\partial x_i}\right) - \rho\langle u_i u_j \rangle\right\} \tag{18}$$

Where δ_{ij} is the kronecker delta (1 for i = j and 0 otherwise), $\langle u_i u_j \rangle$ is refered to as the Reynolds stresses and μ is the viscosity of the fluid.

2.11.2 The Boussinesq approximation

The last term in Eq. (18) is the Reynolds stresses which contain six unknown variables that have to be modeled. This can be done with the Boussinesq approximation where the Reynolds stresses are expressed in terms of the mean velocity. More specifically it is assumed that the turbulent transport of momentum is a diffusive process and can be expressed by a turbulent viscosity, v_T. The Boussinesq approximation reads:

$$-\langle u_i u_j \rangle = v_T \left(\frac{\partial \langle U_i \rangle}{\partial x_j} + \frac{\partial \langle U_j \rangle}{\partial x_i} \right) - \frac{2}{3} k \delta_{ij} \tag{19}$$

Where k is the turbulent kinetic energy per unit mass.

2.11.3 Two equation models

In turbulence modeling based on the Reynolds decomposition and the Boussinesq approximation, the turbulent viscosity, v_T, has to be determined. This can be achieved by defining the turbulent viscosity to be proportional to the product of velocity (u) and length (l) for the large scale turbulent eddies.

$$v_T = C_v u l \tag{20}$$

C_v is a proportionality constant assumed equal for all flows.

In two equation models one transport equation for u and one for l is used to close the Reynolds averaged Navier-Stokes equations, Eq. (18). Other variables correlated to the length and velocity can be used as well. Most common is to use the kinetic energy, k, and the dissipation rate, ε, for the turbulence. The correlations are given in Eq. (21) and (22).

$$l = \frac{k^{3/2}}{\varepsilon} \tag{21}$$

$$u = \sqrt{\frac{2}{3} k} \tag{22}$$

The formulation of the turbulent viscosity based on k and ε is shown in Eq. (23).

$$v_T = C_\mu \frac{k^2}{\varepsilon} \tag{23}$$

Where C_μ is a model constant.

The exact transport equations for k and ε have a lot of unknown terms that has to be modelled. These simplifications will not be shown here.

2.11.4 The standard k- ε model

The modeled equations for k and ε in the standard k-ε model can be seen in Eq. (24) and (25).

$$\frac{\partial k}{\partial t} + \langle U_j \rangle \frac{\partial k}{\partial x_j} = v_T \left[\left(\frac{\partial \langle U_i \rangle}{\partial x_j} + \frac{\partial \langle U_j \rangle}{\partial x_i} \right) \frac{\partial \langle U_i \rangle}{\partial x_j} \right] - \varepsilon + \frac{\partial}{\partial x_j} \left[\left(v + \frac{v_T}{\sigma_k} \right) \frac{\partial k}{\partial x_j} \right] \tag{24}$$

$$\frac{\partial \varepsilon}{\partial t} + \langle U_j \rangle \frac{\partial \varepsilon}{\partial x_j} = C_{\varepsilon 1} \upsilon_T \frac{\varepsilon}{k} \left[\left(\frac{\partial \langle U_i \rangle}{\partial x_j} + \frac{\partial \langle U_j \rangle}{\partial x_i} \right) \frac{\partial \langle U_i \rangle}{\partial x_j} \right] - C_{\varepsilon 2} \frac{\varepsilon^2}{k} + \frac{\partial}{\partial x_j} \left[\left(\upsilon + \frac{\upsilon_T}{\sigma_\varepsilon} \right) \frac{\partial \varepsilon}{\partial x_j} \right] \quad (25)$$

Where σ_k, $C_{\varepsilon 1}$, $C_{\varepsilon 2}$ and σ_ε are constants assumed equal for all flows.

The standard k-ε is robust and the terms in the model are easy to interpret. The model parameters are adjusted for the model to be suited for a wide range of different flows and it has been used extensively in simulations within the field of engineering. It has limitations that should not be ignored [22]. The model was developed for highly turbulent flows (the Reynolds number should be above $50\,000$), isotropic conditions of the turbulent fluctuations and local equilibrium between production and dissipation. Furthermore, it can give bad or even unphysical results for flows with high mean strain rate. It has also been shown to over predict the spreading rate of round jets.

2.11.5 The realizable k- ε model

In the realizable k-ε model the transport equation for turbulent kinetic energy is the same as for the standard k- ε model, Eq. (24), except for the values of the model constants.

An improvement is that C_μ in Eq (23), is no longer constant as it is in the standard k- ε model. Instead it is a function of the flow. This adjustment has been made to make sure the normal stresses, $\langle u_i u_i \rangle$, in Eq. (19), do not reach negative values in flows with large mean strain rates and violates the Schwarz's inequality for the stress tensor.

The transport equation for ε is developed in a different way than for the standard k- ε model. The basis on its development is the dynamic equation of the mean-square vorticity fluctuation.

These modifications have been shown to provide more accurate results for several complex turbulent flows compared with the standard k- ε model [24]. A significant improvement for simulating round jets was one of the most important findings.

2.12 Reactions and mixing

The formation of new molecules through chemical reaction requires certain prerequisites. The laws of thermodynamics determine the final product composition, but do not give any information about how fast the conversion will be.

Reactants have to mix on a large convective scale followed by a small diffusional scale, before collision of individual molecules can take place. The relative importance of the mixing and the molecular kinetics for the overall reaction rate can be quantified by the Dahmköhler number [22], Da.

$$Da = \frac{Typical\ time\ required\ for\ mixing}{Typical\ time\ required\ for\ chemical\ reactions} \quad (26)$$

Chemical reactions on the molecular level can be complex and consist of many reaction steps. It is important to understand the mechanisms. In [25] reaction schemes for several species including hydrogen, methane and higher hydrocarbons are presented. The large amount of reaction steps and intermediate species requires simplifications for the modelling of complex systems.

In many studies the rate constant is expressed as in Eq. (27) [26].

$$k = AT^n \exp(^{-E}/_{RT}) \tag{27}$$

Where A *is* the kinetic pre-exponetial factor, E is the activation energy and T^n accounts for the temperature dependence of A.

It is clear from Eq. (27) that reaction rates increase fast with temperature. This temperature dependence is suitable for reactions with mechanisms according to Arrhenius and transition state theory, which are important for combustion. Recombination of radicals, however, shows a different temperature dependence [26].

The typical time of chemical reaction can be estimated as the time to completely consume the limiting reactant [22]. This requires knowledge of the rate constant, the reaction order and the concentrations of the reactants.

Mixing can be described as the process in which a non-homogeneous mixture is transformed to a homogeneous mixture. This takes place on a macro level and on a micro level [22]. The macro mixing is the distribution of the species over the whole domain by the mean flow and the largest scales of the turbulence. From here on, micro mixing reduces the size of fluid elements until diffusion creates a complete homogeneous mixture on the molecular level. This latter process includes stretching and deformation by the turbulent vortices followed by similar effects from viscous forces. The result is increased surface area between fluid elements to a point where diffusion will take over as the dominating mixing process.

According to [22], the typical time for mixing can for most cases be estimated as the time scale of the largest micro mixing scale, Eq. (28), i.e. the deformation and stretching of the fluid elements from the turbulence.

$$Typical\ time\ for\ mixing = 0.5\frac{k}{\varepsilon} \tag{28}$$

Where k and ε are the turbulent kinetic energy and the dissipation rate respectively.

When the Dahmköhler number is much larger than one the reaction rate can be considered as instantaneous compared to the mixing rate. A modelling approach for this specific case is presented in the following sections.

2.12.1 Mixture fraction

The mixture fraction, ξ, for a two-inlet situation is defined as

$$\xi_i = \frac{Z_i - Z_{i,1}}{Z_{i,2} - Z_{i,1}} \tag{29}$$

Where Z is the elemental mass fraction. The index i corresponds to the element. The two inlets are referred to by 1 and 2.

The elemental mass fraction is defined as

$$Z_i = \frac{Mass\ of\ element\ i}{Total\ mass} \tag{30}$$

If the diffusivities are equal for all the species the mixture fraction will be independent on the individual elements and can be a measure of how the mixing progresses downstream from the two inlets. The mixture fraction takes different values between 0 and 1 indicating how much in the mixture that originated from each inlet. Unlike species, elements are not created or destroyed in reactions; this ensures that the mixture fraction is a conserved scalar. ξ is therefore very useful for modelling reactions where mixing rate limits the reaction [27].

2.12.2 β-PDF

In turbulent flows at different positions the mixture fraction will fluctuate in time at values between 0 and 1 due to the turbulence. This can be visualized by a probability density function (PDF). An example of the fluctuations in time and the corresponding PDF is illustrated in Figure 3.

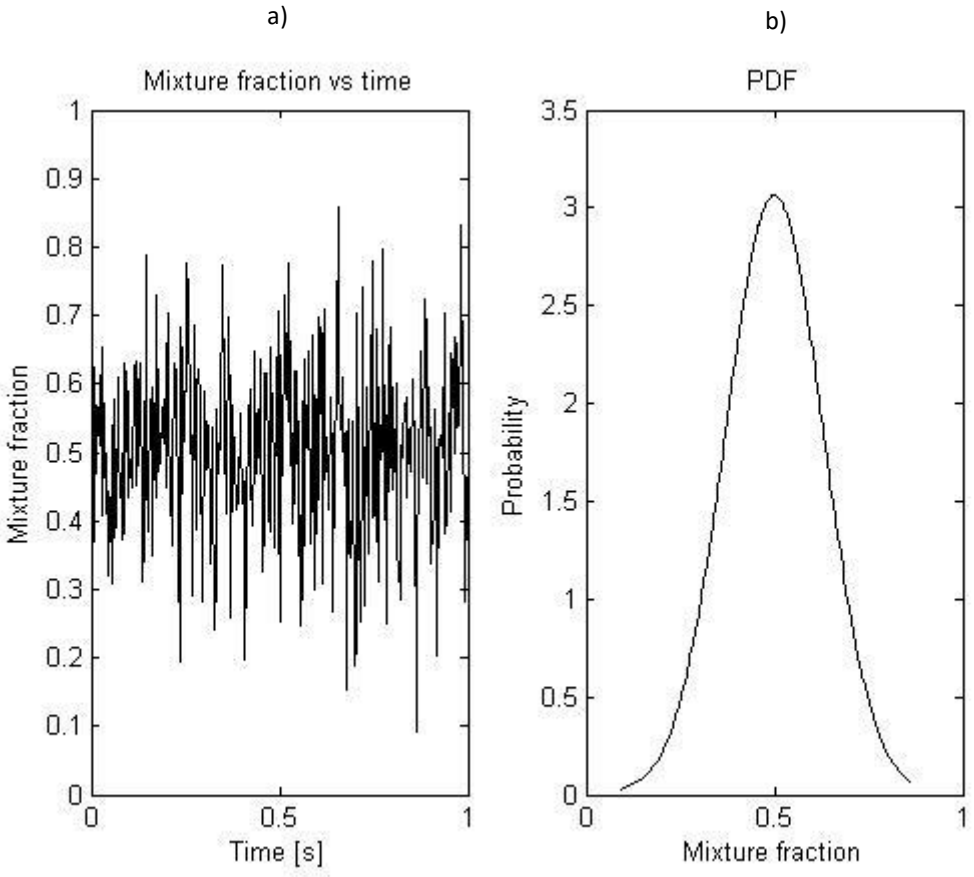

Figure 3. a) The fluctuations of the mixture fraction at a certain position due to turbulence and b) the corresponding probability density function, adopted from [22].

The instantaneous mixture fraction,ξ, can then be represented statistically by the mean mixture fraction $\langle\xi\rangle$ and the mixture fraction variance σ^2 [22]. $\langle\xi\rangle$ represents the macro scale mixing and σ^2 corresponds to the micro scale mixing. As σ^2 approaches zero the flow approaches homogeneity.

By solving transport equations for the mean mixture fraction and the variance a model for the PDF can be obtained, which represents the real mixture fraction. A common way is to use the β-PDF [22].

The transport equations for $\langle\xi\rangle$ and σ^2 including closure terms are [28].

$$\frac{\partial\langle\xi\rangle}{\partial t} + \langle U_j\rangle\frac{\partial\langle\xi\rangle}{\partial x_j} = \frac{\partial}{\partial x_j}\left[\left(\frac{\upsilon + \upsilon_T}{\sigma_t}\right)\frac{\partial\langle\xi\rangle}{\partial x_j}\right] \tag{31}$$

$$\frac{\partial\sigma^2}{\partial t} + \langle U_j\rangle\frac{\partial\sigma^2}{\partial x_j} = \frac{\partial}{\partial x_j}\left[\left(\frac{\upsilon + \upsilon_T}{\sigma_t}\right)\frac{\partial\sigma^2}{\partial x_j}\right] + C_g\upsilon_T\frac{\partial\langle\xi\rangle\partial\langle\xi\rangle}{\partial x_j\partial x_j} - C_d\frac{\varepsilon}{k}\sigma^2 \tag{32}$$

Where σ_t, C_g and C_d are model constants.

2.12.3 Look up table

For the assumptions that equilibrium is achieved as soon as the reactants mix, the species have the same constant diffusivities, the diffusion of heat in the fluid has the same rate as the diffusion of species (i.e. a Lewis number of unity) and that there are adiabatic conditions, then some important variables can be expressed by the mixture fraction alone [27]. These variables are the concentrations of the species, the temperature and the density. To save computational time these variables can be calculated prior to the CFD calculations and stored in a "look-up table". This look-up table then consists of the concentrations, the temperature and the density at all the possible combinations of $\langle\xi\rangle$ and σ^2 [22].

3 Method

The overall approach was to compare the actual data with the design data. Since the design data had a lower fuel consumption, it was used as a reference case. In this work the plant data was analyzed by several methods, presented below, including CFD simulations of the combustion process.

3.1 Data gathering & mass balance calculations

The design data is quite old since the plant was built in 1978. The data referred to as actual data was taken from operational conditions on the 6^{th} of March 2015. Some data were measured directly in the process and could be extracted from monitoring screens in the control room and some data had to be calculated with mass balances based on other streams. Compositions of relevant streams were obtained from gas chromatography analysis. This gives the compositions in dry basis and some additional mass balance calculations had to be performed to include the amount of water in the different streams. Unlike the other streams the composition of the heavy hydrocarbon gas was based on an older measurement from 12^{th} of September 2014.

The amount of air for the combustion process is not measured directly during normal operation of the primary reformer. It is instead controlled manually by increasing or decreasing the inlet area. For the design data $15\ \%$ excess of air was assumed, based on the design specification from the plant manufacturer. The amount of air for the actual data was calculated to $16.3\ \%$ excess. This calculation was based on the assumption of complete combustion and a gas chromatography analysis of the composition of carbon dioxide and oxygen in the flue gas at the outlet of the radiant section. The assumption of complete combustion was later verified by another gas chromatography analysis at the outlet of radiant section, performed by the company, in which no indication of methane, hydrogen or carbon monoxide could be found.

3.2 Energy balance and adiabatic flame temperature

An energy balance was calculated over the radiant section for both actual and design data. These calculations included the heat release from the combustion of the fuel, the energy used to heat up the flue gases to the outlet temperature and the energy used for the steam reforming inside the tubes. Based on the energy balance, losses and the possible energy savings could be analyzed.

Additionally, the adiabatic flame temperature was calculated for actual and design data for comparison. The fuel composition was also varied in several ways (see the result section) for which the adiabatic flame temperature was calculated as well; with the aim of finding possibilities of increased heat transfer with less consumption of natural gas.

Thermodynamic data was taken from NIST [29] and atmospheric pressure was assumed since the furnace is connected to the atmosphere through peep holes (see the picture on the front page). Integration of the polynomials for the highly temperature dependent values for the specific heat capacities was performed in MatLab®.

3.3 CFD

3.3.1 Geometry

One of the 200 burners can be seen in Figure 4. The numbers, $1-3$ correspond to fuel inlet, primary air inlet and secondary air inlet, respectively. Pre-mixing of fuel with primary air takes place in the upper part of the burner. At the lower end secondary air is introduced, which is where the combustion takes place. It

was chosen to set the boundaries for the geometry where the pre-mixed fuel and the secondary air enters the domain, i.e. the lower part of the burner.

Figure 4.One of the 200 burners in the primary reformer. The fuel enters in the top (1), is pre-mixed with primary air (2) and finally the premixed fuel mixes with secondary air and combustion takes place (3).

A photo taken from the bottom of the furnace can be seen in Figure 5 a). The rows of tubes with rows of burners in between are highlighted with red arrows. To reduce the size of the domain and thereby obtain reasonable computational times symmetry conditions were used. The symmetry chosen is shown in Figure 5 b). As can be seen in the figure, the geometry then included one fourth of a burner and half of a tube. This symmetry can be motivated for most parts of the furnace, but it is not representative close to the walls. Limitations due to the symmetry should be kept in mind. Effects from the hot furnace walls and any uneven fluctuations between different parts of the furnace will not be revealed.

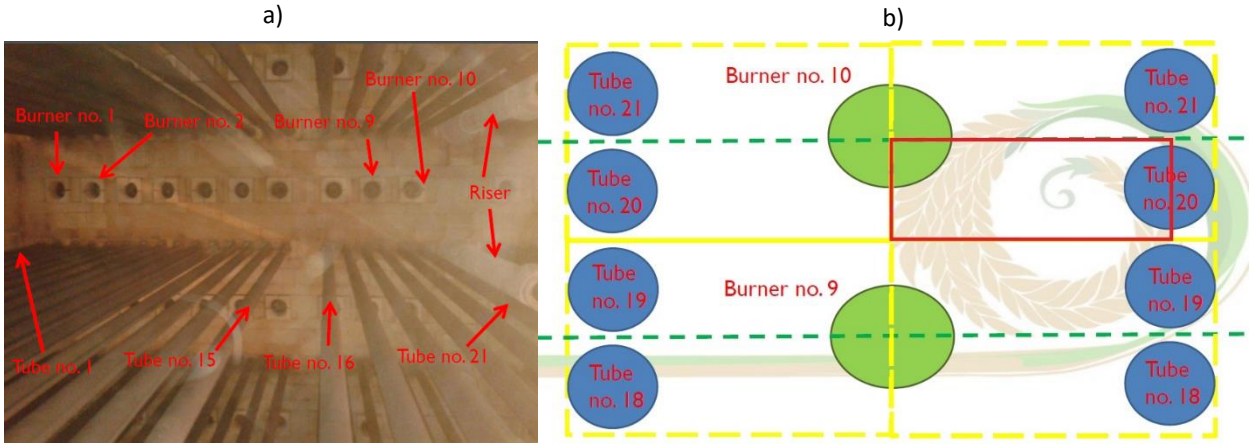

Figure 5. a) Picture taken from the bottom of the furnace. b) Illustration of the symmetry, marked with a red rectangle, used for the geometry.

To make sure to capture the whole combustion process $80\ \%$ of the furnace was included, i.e. $8\ m$ of the $10\ m$ high furnace. The final CAD geometry is shown in Figure 6. To be able to use the symmetry boundary condition the number of inlets for the secondary air was changed from 7 to 8, which meant that two inlets

were included in the geometry due to the symmetry condition. The total inlet area, however, was kept constant. This area was the maximum area when the inlets were completely open.

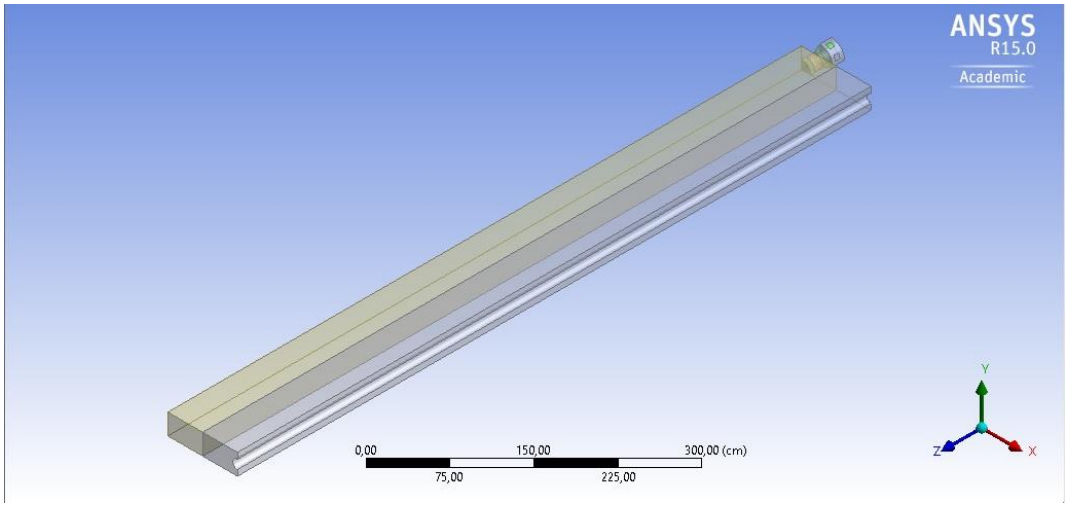

Figure 6.The geometry used to simulate the combustion process in the primary reformer.

For symmetry reasons the number of holes in the perforated plate where the pre-mixed fuel enters the domain was changed from 31 to 29, but the total inlet area was kept here as well. A picture of the fuel inlet and a closer look at the CAD geometry of this part can be seen in Figure 7. A short distance downstream of the fuel inlet there is a small extension of the walls, which can be seen in the figure. It was believed that the main function of this extension was to create turbulence. To reduce the number of cells and thereby reduce computational time the wall extension was neglected. The motivation for this is that the turbulence at the inlet was not known and had to be estimated and tested with a sensitivity analysis anyway.

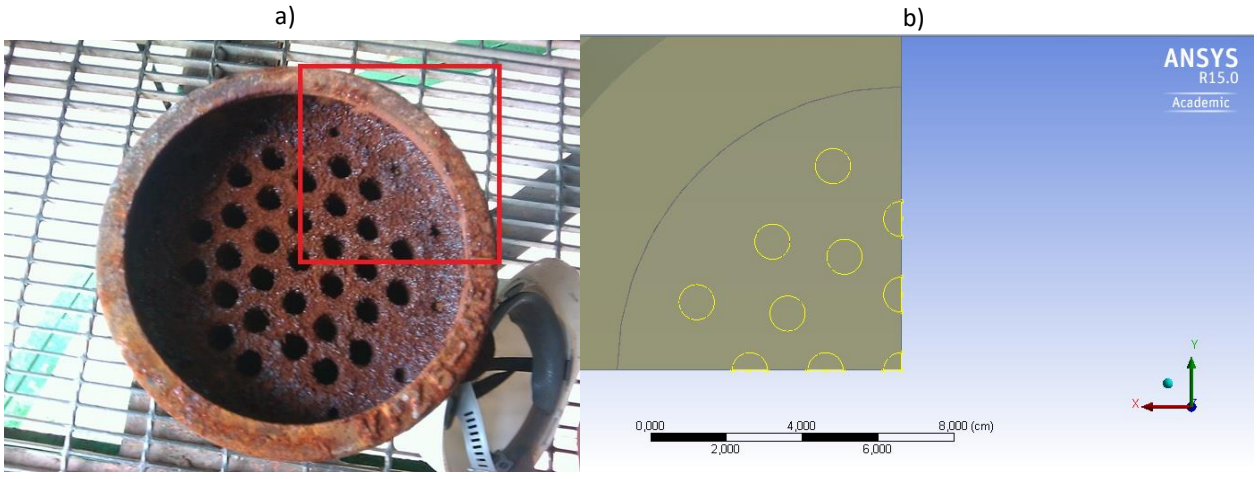

Figure 7. a) Picture of the perforated plate through which the pre-mixed fuel enters the domain for combustion with secondary air. b) The slightly simplified geometry of the fuel inlet.

3.3.2 Mesh

The geometry was complex and therefore the mesh was created by tetrahedral elements. Since the largest gradients could be expected closer to the inlets the cells were made smaller in that region. At the walls

inflations with 5 layers were used. The walls closer to the air inlet was made with 3 layers. The first layer thickness was initially estimated by the wall stresses and after a converged solution the y+ values were checked to lie within appropriate ranges.

To see how much the mesh affected the solution three meshes with increasing number of cells were used. One consisting of approximately $140\,000$ cells, one with approximately $240\,000$ cells and one with approximately $380\,000$ cells.

The quality of the mesh and the mesh elements were within best practice guidelines, except a few outliers. The overall mesh was judged as good. To quantify the mesh quality the values for the aspect ratio, orthogonal quality and the skewness can be seen in Table 1 for the mesh with the highest density. The other two meshes were of similar quality.

Table 1. The quality of the mesh with highest density.

	Min	Max	Average
Aspect ratio	1.16	14.54	2.64
Orthogonal quality	0.18	1.00	0.87
Skewness	2^{-4}	0.94	0.24

3.3.3 Models

The realizable k-ε model was chosen to account for the turbulence, due to its suitability for swirling flows, adverse pressure gradients and round jets. All these factors were expected in the system based on the geometry and the round nozzels of the fuel inlet. The Reynolds number was calculated at three different locations in the opening between the burner and the furnace, the part where the mixing is most significant. All three numbers were much higher than $50\,000$ showing that the flow is strongly turbulent. This does not ensure that the flow is highly turbulent in other parts of the geometry, but since a large amount of energy is released by combustion it is reasonable to assume that the turbulence is sustained through most part of the geometry.

The non-equilibrium wall function was used to obtain the boundary conditions for velocity and turbulent properties at the walls. Impingement on the burner wall from the air inlet was expected as well as swirling flow in the burner region and in the upper part of the furnace. Therefore, deviations from the equilibrium assumption had to be accounted for.

The non-premixed combustion model was used to account for the reactions. To simplify the situation, and since the ratio between primary air and secondary air was unknown, all air was assumed to enter the domain as secondary air. This is expected to show a slower combustion than reality. The very high temperatures of the flames (above $2000\ K$) motivates the assumption of neglecting the kinetics since the reaction rates at such high temperatures are very fast and thus the situation can be reduced to a mixing problem.

The simulations were run as adiabatic, excluding the heat transfer to the tubes. This means that the simulations will show significantly higher temperatures than in reality. The results can be considered as showing the combustion in the primary reformer without the reforming reactions in the tubes. It should be kept in mind that neglecting the heat transfer will have an impact on the behavior of the combustion since some fluid properties are functions of the temperature.

3.3.4 Setup

Mass flow inlet was chosen as inlet condition, which gives the mass flow as a fixed value, while velocity is calculated based on the density and inlet area. The mass flow, temperature and composition of fuel and air was set according to the process data. Only the main species involved in the reactions were included in the equilibrium calculations since e.g. radicals were not of interest in the analysis.

The values of the turbulent properties had a high uncertainty. Turbulent intensity was estimated based on the assumption of fully developed turbulent pipe flow. According to [22] the turbulent intensity (I) and the turbulent length scale (L) was estimated from Eq. (33) and Eq. (34) respectively. This assumption is reasonable for the fuel inlet with a pipe upstream, but is questionable for the air inlet since it is an opening directly to the atmosphere. For this reason, a sensitivity analysis was performed for the turbulence properties at the inlets.

$$I = 0.16Re^{-1/8} \tag{33}$$

$$l = 0.07 * L \tag{34}$$

Where L is the hydraulic diameter.

In Table 2 the settings for the actual and design simulations are summarized. The compositions of the different streams can be found in Table 6 in Appendix B.

Table 2. Inlet conditions for simulations of actual and design data.

	Actual		**Design**	
	Fuel inlet	**Air inlet**	**Fuel inlet**	**Air inlet**
m [kgs^{-1}]	0.00707	0.0918	0.00651	0.0829
T [K]	414.15	303.15	338.7	303.15
$\langle\xi\rangle$	1	0	1	0
σ^2	0	0	0	0
I [%]	5.2	4.2	5.2	4.2
L [m]	0.0093	0.056	0.0093	0.056

The outlet was defined as “outflow”, which is a boundary condition that extrapolates the values from the interior solution. Using outflow requires the placement of the outlet at a position where the variables no longer change in the flow direction or at least far away from the region of interest so it does not affect the solution. This was considered fulfilled for these simulations since the combustion would be finalized at the outlet.

The operating pressure was set as atmospheric which was judged as reasonable due to the connection between the furnace and the atmosphere through the peep holes (see the picture on the front page). Built in polynomials for temperature dependence of the specific heat for the different species were used. The viscosity was set at a constant value for all the species. This is considered an acceptable approximation

due to the high turbulence of the flow for which the viscous transport at the molecular level can be regarded as negligible.

A discretization scheme accounting for the transportiveness was applied. The equations were solved with the SIMPLE algorithm at steady state conditions. Judging convergence was based on monitoring the residuals of all the variables, observing the stability of the variables at certain locations and checking the overall mass balance of the solutions.

4 Results and analysis

This section consists of three parts: Energy balance, adiabatic flame temperature and CFD. These parts are related to the questions presented in the objectives. The part named energy balance should be read with the question about possible energy improvements in mind. The part named adiabatic flame temperature is related to the two questions regarding fuel composition and flame temperature. Finally, the part named CFD concerns the last question in the objective, i.e. a comparison of design and actual data in respect to the mixing of fuel and oxidizer.

4.1 Energy balance

The result from the energy balance calculation over the radiant section is presented in Figure 8, where the actual condition (A) is compared with the design condition (D). As stated by the company it is clear that there is a higher amount of heat used for the combustion (approximately 10% higher). The heat supplied to the reforming reaction in the tubes are almost the same. The energy leaving radiant section to convective section for heat recovery is approximately 8% higher. A reduction of this would mean less fuel needed, but since the temperature of the flue gases leaving to the atmosphere is similar, it seems as this heat is needed in the convective section. Finally, when subtracting "heat to tubes" and "flue gases" from "fuel", the losses are obtained. The losses are much higher ($17.3\ MW$ compared to $6.0\ MW$) and the losses per fuel is 4% for design conditions and 9% for actual conditions. By reducing the losses it should be possible to reduce the fuel consumption. The reason behind the higher losses is unfortunately unknown. Looking at the whole system and assuming that the temperature of the flue gases leaving to atmosphere ($450K$-$500K$) is the minimal, one can conclude that the overall efficiency of the primary reformer is $96.4\ \%$ for design data and $90.7\ \%$ for actual data.

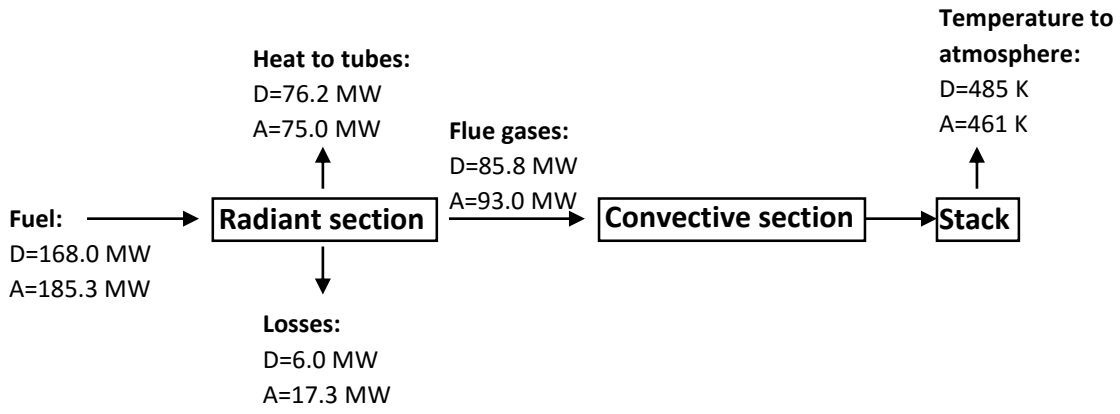

Figure 8. Schematic of the energy balance calculation over radiant section of primary reformer for design data (D) and actual data (A). The temperature of the flue gases leaving to atmosphere after passing through convective section is also included in the figure.

4.2 Adiabatic flame temperature

The adiabatic flame temperature for combustion of the fuel was calculated to $2104.77\ K$ for the design data and $2105.48\ K$ for the actual data, i.e. almost exactly the same temperature for the two cases. Obviously, the amount of fuel has not been increased to raise the temperature of the flame. This does however not exclude that there is a higher heat transfer resistance, e.g. due to fouling, that is the cause of the higher fuel consumption.

To see how the flame temperature varies with the fuel composition the adiabatic flame temperature was calculated for different fuel compositions. The amount of tail gas and natural gas in the actual fuel was varied while the amount of heavy hydrocarbon gas was kept constant, see Appendix A for the fuel streams. The main idea was to reduce the amount of natural gas and at the same time increase the flame temperature to keep or improve the heat transfer efficiency. How the flow rate of natural gas and tail gas was changed in these calculations is presented in Table 3.

The results from these calculations can be seen in Figure 9. The x-axis represents the amount of tail gas in percentage compared to the actual amount. The circles represent a reduction of natural gas by 50 % and the squares a reduction of natural gas by 25 %. The diamond and the triangle represents the actual and the design adiabatic flame temperature respectively.

It is clear that increasing the amount of tail gas reduces the adiabatic flame temperature. When the amount of tail gas is unchanged (100 %) and the amount of natural gas is reduced (50 % & 75 %) the adiabatic flame temperature is lowered. If the amount of tail gas is reduced the amount of natural gas can also be reduced without lowering the adiabatic flame temperature. In fact, the temperature is increased, which should lead to a higher heat transfer rate.

Table 3. Evaluation matrix for the gas composition.

Amount of natural gas compared to actual amount [%]	Amount of tail gas compared to actual amount [%]
50	50
50	75
50	100
75	50
75	75
75	100

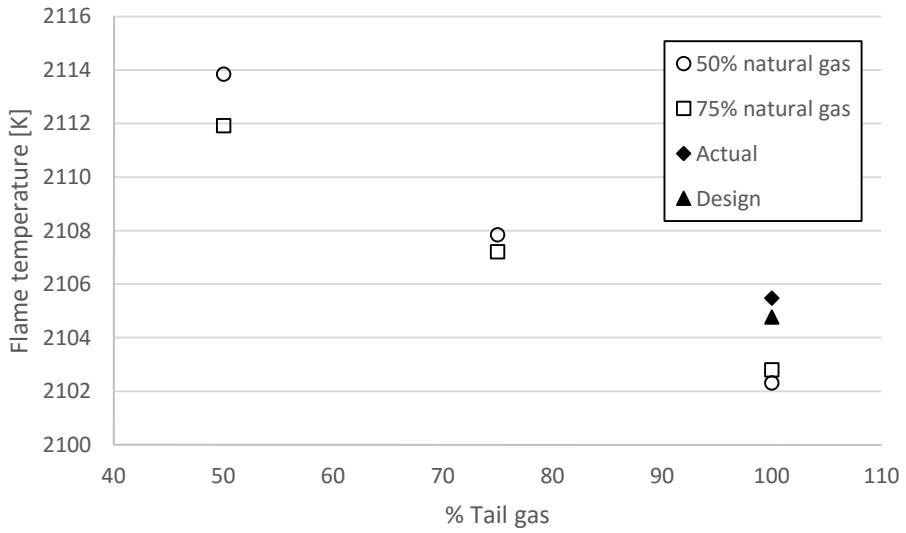

Figure 9. The adiabatic flame temperature for combustion of fuel with different compositions.

One can unfortunately not only look at the temperature of the flame. The amount of energy in the fuel also has to be taken into account. A certain heat load is needed both for the reforming reactions and for the convective section. Since all the investigated cases had a lowered total mass flow rate compared to the original case, this had to be checked. To see whether the fuel compositions in Table 3 contained enough energy, a calculation of the fuel heating value was performed. The results are presented in Figure 10. The x-axis represents the amount of tail gas in percentage compared to the actual amount. The squares represent a reduction of natural gas by $50\ \%$ and the circles a reduction of natural gas by $25\ \%$. The fuel heating value for design and actual data is also included in the figure. It is clear that the amount of energy is not enough in neither of the cases since all of them has a lower heating value than both design and actual fuel.

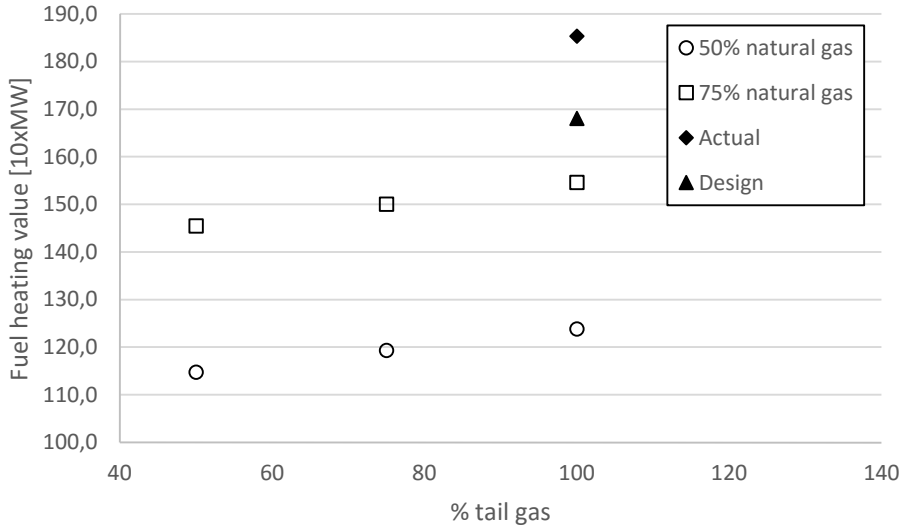

Figure 10. The fuel heating value for combustion of fuel with different compositions.

A smaller reduction of natural gas and tail gas (less than 25%) than examined here would of course lead to higher fuel heating value comparable to the design fuel. In that case the heat load could possibly be sufficient. But looking at Figure 9 it can be seen that the value of the adiabatic flame temperature will approach the temperature of the design and actual fuel. Unless the adiabatic flame temperature is significantly higher it cannot compensate for a lower flow rate. Additionally, increasing heat transfer by raising the flame temperature is questionable since it will put higher demand on the tube wall material and thus their service life time might be reduced.

4.3 CFD simulations

4.3.1 Grid independence

To evaluate how the solutions were affected by the density of the mesh a grid independence test was executed. A plot was made showing how the fuel was consumed as the flue gases moved towards the outlet. The dependence was tested by comparing the simulation results for three meshes with increasing amount of cells. One with $140\ 000$, one with $240\ 000$ and one with $380\ 000$ cells. The plot is shown in Figure 11. In Appendix C the method for calculating the fuel consumption is described. The solutions are not grid independent, but it can be seen that there are sufficient amount of cells to not affect the solution too much. Since the basis of the analysis was of a comparative nature and the same mesh was used for all

the simulations, it was decided to use the grid with $240\,000$ cells. This decision lead to reasonable computational times making it possible to simulate more cases.

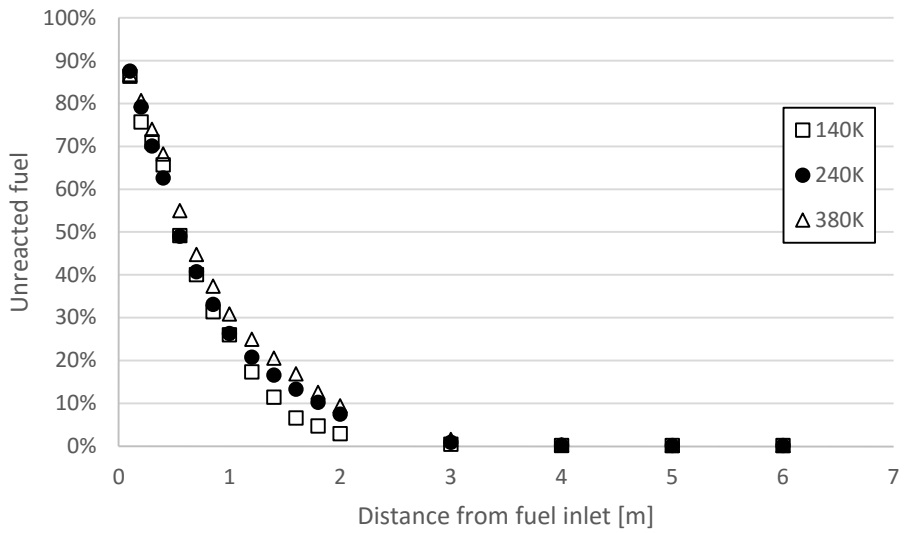

Figure 11. Grid independence test.

4.3.2 Effect of turbulence

Since turbulence is important for mixing and since the magnitude of the turbulence was unknown at the inlets a sensitivity analysis was performed to see what effect the estimated turbulence would have on the solution. The values for the turbulent intensity, I, at the air inlet and at the fuel inlet were altered from the original estimated values for the actual case. In Table 4 a matrix showing the variations of turbulent intensity in the four studied cases ($A1 - A4$) is presented. The turbulent intensities were halved or doubled. A doubling of the intensity leads to an increase of k and ε by a factor 4 and 8, respectively. Halving the intensity, on the other hand, means that k and ε decrase by a factor 4 and 8, respectively.

Table 4. The changes of turbulent intensity, I, for the sensitivity analysis .

	Air inlet		**Fuel inlet**	
	***I* [%]**	***L* [m]**	***I* [%]**	***L* [m]**
Actual	4.2	0.056	5.2	0.0093
A1			2.6	
A2			10.4	
A3	8.4			
A4	2.1			

The results from the turbulence sensitivity analysis for fuel and air inlet are presented in Figure 12 and Figure 13. Fuel consumption is plotted against the distance from the fuel inlet. In Appendix C the method for calculating the fuel consumption is described. The combustion is nearly unaffected by the change of turbulent properties at the inlets, since the markers in the figure are almost on top of each other. It is believed that turbulence is produced to a much higher degree inside the geometry which makes the simulations relatively insensitive to the amount of turbulence entering the domain.

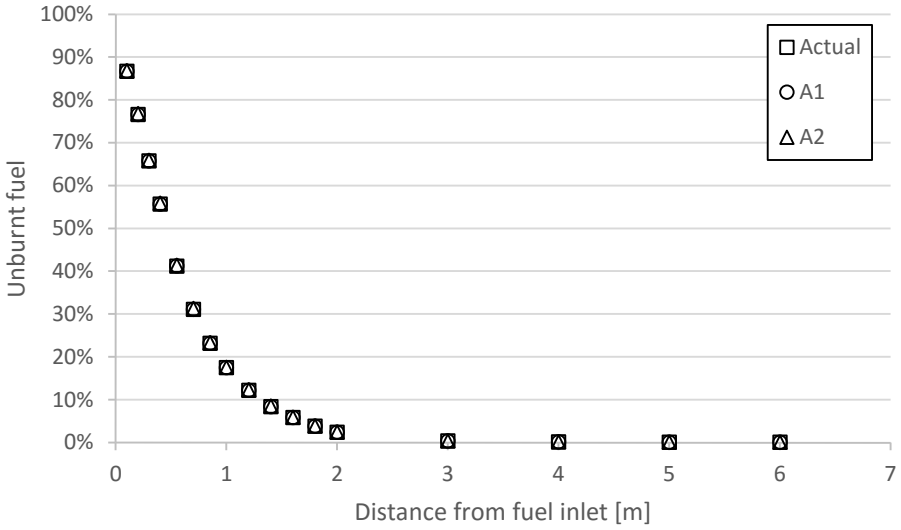

Figure 12. Turbulence sensitivity analysis for fuel inlet.

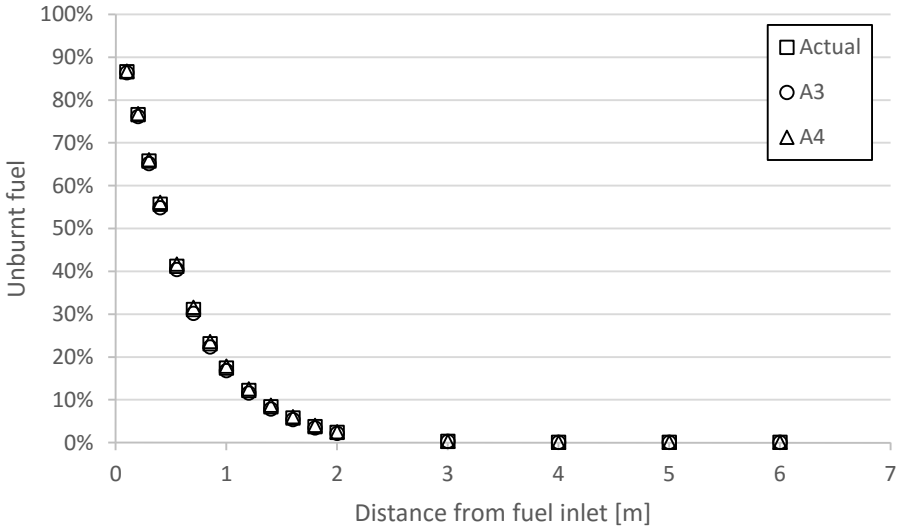

Figure 13. Turbulence sensitivity analysis for air inlet.

A simulation was also run with the *standard* k- ε *model* and the *standard wall function* to compare the effect of the modelling approach of the turbulence. In Figure 14 the simulation result is compared with the results from the original simulation, in which the realizable k- ε *model* and the non-equilibrium wall function was used. It can be seen that there is a difference between the two and that the realizable k- ε model along with non-equilibrium wall function predicts a faster combustion. A difference plot is included in the figure and the values can be found on the axis to the right. The maximum difference occurs at approximately $0.75\ m$ from the fuel inlet where almost 3 percentage of the fuel additionally has been consumed.

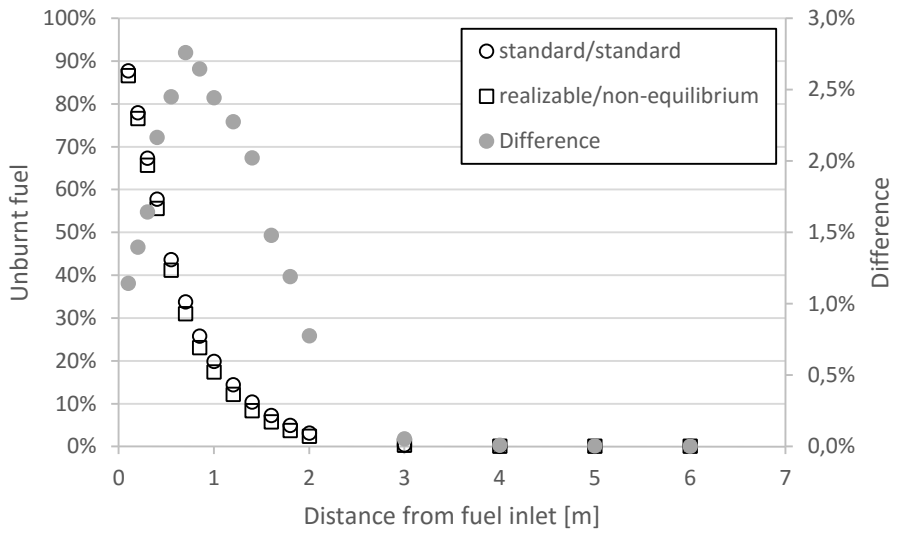

Figure 14. Comparison of two simulations with different turbulence model and wall function.

It can be concluded that the choice of turbulence model has a much bigger impact on the solution than the turbulent boundary conditions. The *realizable k-ε turbulence model and the non-equilibrium wall function* was judged as the best choice for these simulations, but a deeper evaluation could be a good idea for future studies.

4.3.3 Design vs actual

In order to obtain better understanding of why the fuel consumption differs so much between the design data and the actual data the simulation of the design data was compared with the simulation of the actual data.

In Figure 15 the fuel consumption for the two cases are compared as the combustion process progresses away from the fuel inlet. The method for calculating the fuel consumption is described in Appendix C. It can be seen that the combustion is faster in the actual case than in the design case. A difference plot is included in the figure and the values are shown on the axis to the right. The maximum difference takes place $1\ m$ from the fuel inlet where close to 6 percentage more of the fuel has combusted. It is in the upper half of the furnace where the difference can be seen. In the lower part all the fuel has reacted. The more efficient combustion for the actual data can be explained by the higher flow rate, which creates more turbulence and thus increases the mixing rate.

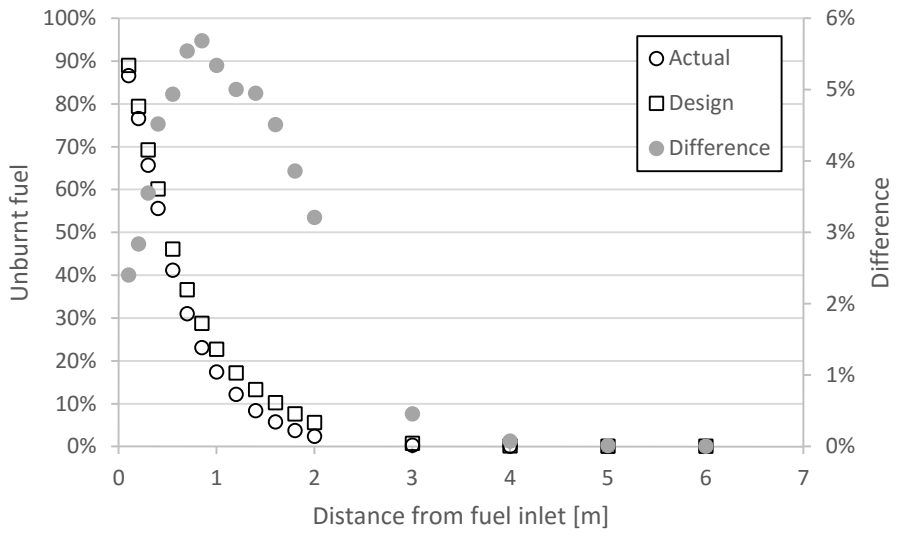

Figure 15.Comparison of the simulation results with the design data and the actual data.

A feature that could be seen in the simulation results for both design and actual data was recirculation of the combustion gases in the upper part of the furnace. This is shown in Figure 16, where the velocity vectors for the actual data is plotted on a plane. Recirculation of this kind is believed to be of high importance for the combustion. The reason for this is that unreacted fuel and air can travel back into the flame zone creating stability to the flame and making the combustion relatively insensitive to instabilities at the inlet conditions.

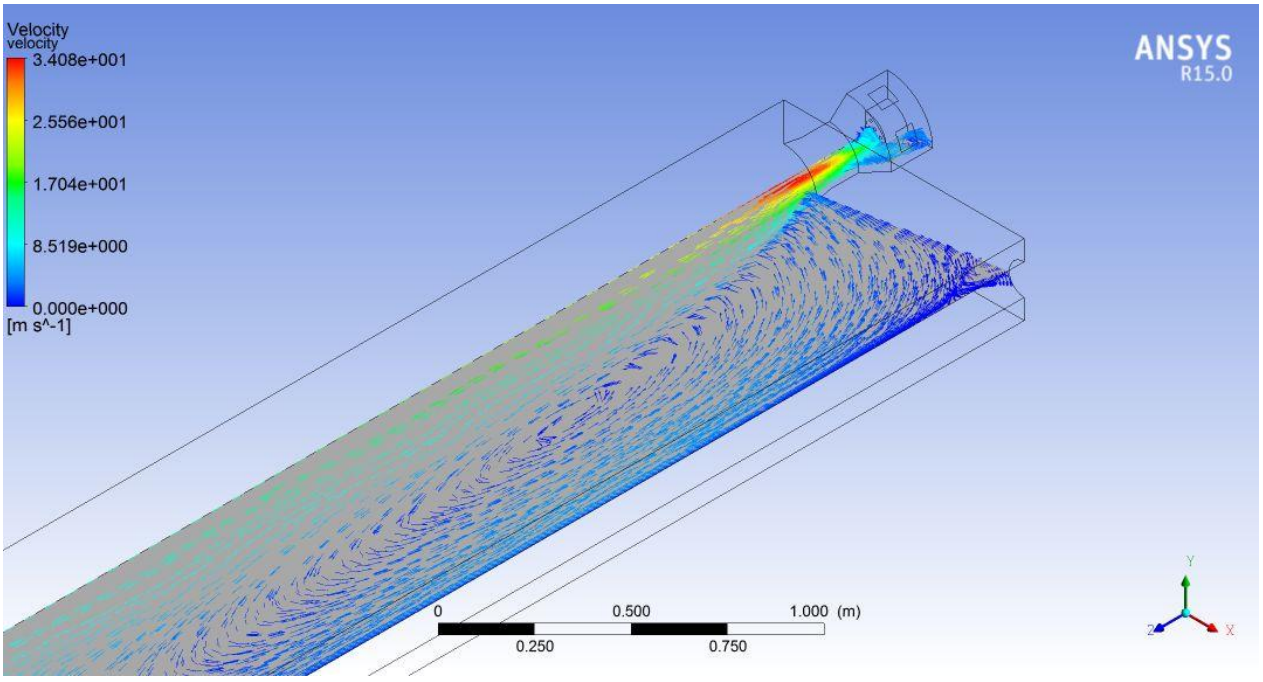

Figure 16. Velocity vectors for the actual case.

It is important to compare the temperature, since the temperature difference between the flame and the tube wall is the main driving force for the heat transfer. Higher flame temperatures lead to better heat transfer, but might have a destructive impact on the tube material if too high temperatures reach the tube walls. Given the right fuel composition along with correct flow rates of fuel and air, a fast combustion should be the optimal situation since it would enable an efficient heat transfer already in the upper part of the furnace.

Before the temperature is analyzed the implications from the assumption of adiabatic conditions have to be discussed. In the real scenario continuous heat transfer, mainly by radiation, from the flames to the tubes occur. This means that the temperature in the furnace is lowered as the combustion gases moves towards the bottom of the furnace. That is not the case in these simulations. This can be seen in Figure 17, in which the temperature profile for the actual case is plotted on a plane. Due to the adiabatic condition and the recirculation a higher temperature than expected is obtained in the upper part and in the lower part of the furnace. The mixing zone, however, should be less affected by these simplifications.

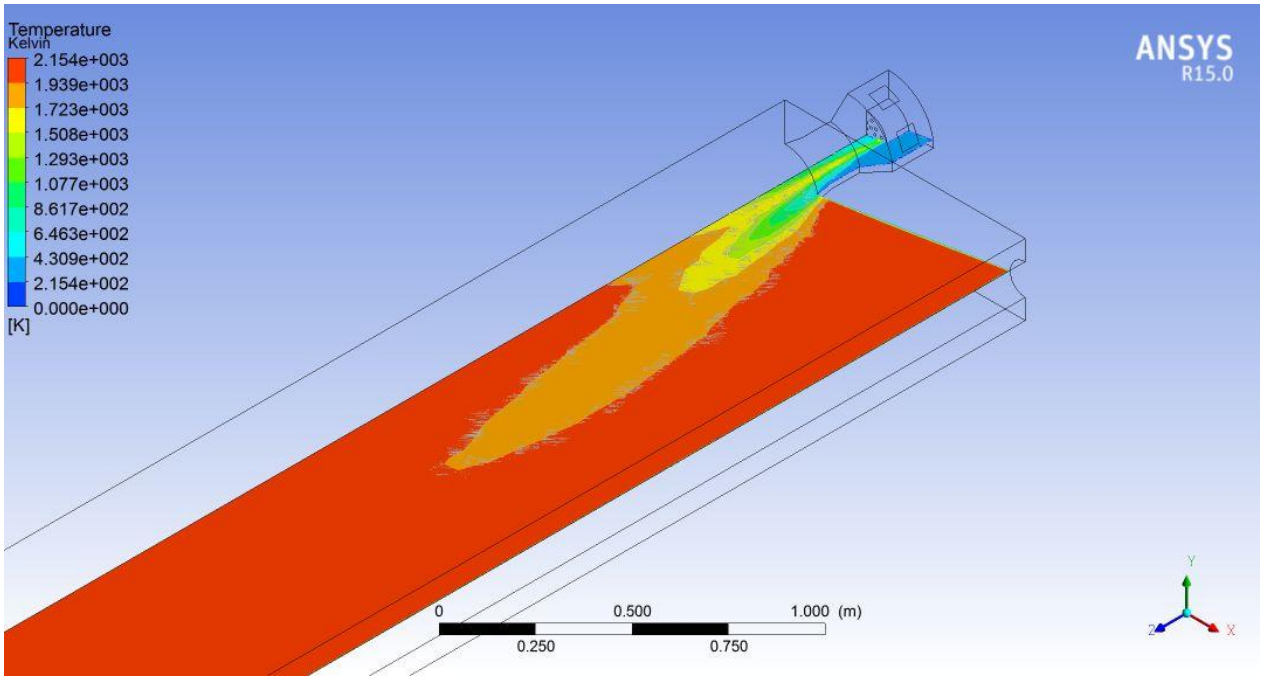

Figure 17. Temperature profile for the actual case.

The temperature at different positions in the furnace downstream of the fuel inlet for actual and design data is plotted in Figure 18. This temperature was calculated with an averaging procedure described in Eq. (35) to mitigate the effect from the recirculated combustion gases and the adiabatic condition.

$$T = \frac{\dot{m}T + abs(\dot{m})T}{2(\dot{m}+abs(\dot{m}))} \tag{35}$$

Where $\dot{m}$ is the mass flow rate.

In Figure 18 it can be seen that the flame temperature increases faster for the actual data than for the design data in the upper part of the furnace. After some distance, however, the similar adiabatic temperature is reached for both cases. The difference is plotted as well and the values are presented on

the axis to the right. The maximum temperature difference is around $70\ K$ and there is a sharp distinction after $2\ m$ where the difference evens out.

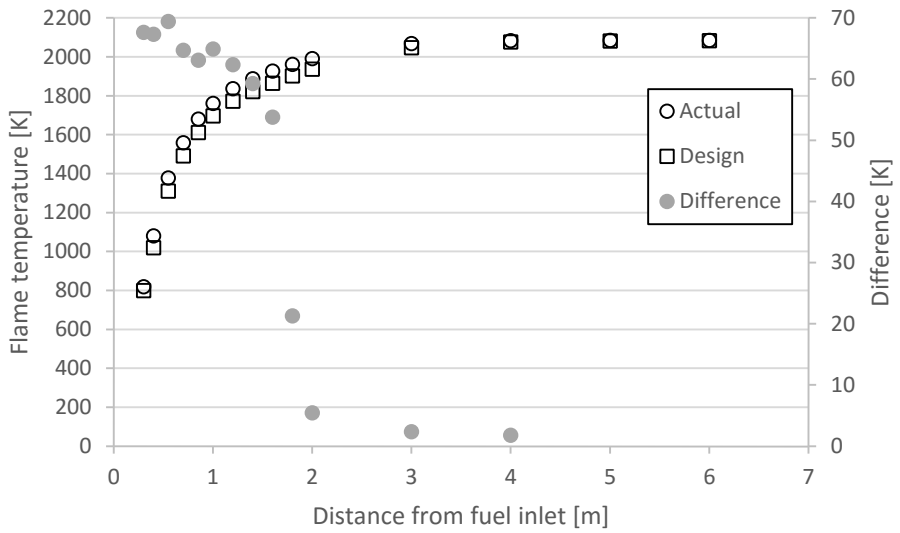

Figure 18. Comparison of flame temperature development for design and actual data.

The faster combustion due to increased turbulence that was seen in Figure 15 resulted in a higher temperature in the upper part of the furnace for the actual data than for the design data. It can therefore be speculated that the flow rate was increased to obtain a more efficient combustion. If so, the reason why this was necessary remains unknown. However, the temperature difference is quite low and it is difficult to say to what extent it impacts the heat transfer and if this effect is significant compared to other parameters that was not included in these simulations.

5 Discussion

The adiabatic flame temperature for design data and actual data is almost the same. The simulations did show a higher temperature for the actual data due to better mixing in the upper part of the furnace. This temperature difference is however quite small. Additionally, there are several simplifications and uncertainties that makes it difficult to draw any reliable conclusions from this result. The most important limitations are that pre-mixing and heat transfer were neglected. Another limitation is that the simulations were not independent of the grid.

Even if the actual conditions has improved the mixing and thereby the combustion process it doesn't really explain why there is a higher fuel consumption. It should mainly be considered as a positive effect. The main difference between design and actual data is still the higher flow rate of the actual data, i.e. more fuel and more air. Unfortunately, this brings us back to the original problem of identifying why this is so. There are four possibilities that could explain why the fuel consumption has increased. These will be presented and discussed here.

The first possibility is that there is insufficient mixing of fuel and oxidizer. This could lead to unreacted fuel leaving the radiant section. A gas chromatography analysis was executed to rule out this explanation. Insufficient mixing could still be an issue if the combustion is delayed. This situation is illustrated in Figure 19. In the optimal combustion process all fuel has reacted so that all heat is released before the combustion gases enter the furnace. Then the temperature is at the maximum value and the heat transfer rate will be as high as possible directly and the heat will have plenty of time to be transferred to the tubes. If, however, the combustion is delayed, then the temperature will not be at its maximum value directly at the entrance of the furnace. The heat transfer rate will then be lower initially and less heat will have time to be transferred to the tubes during the same residence time. This could be compensated for by a higher flow rate. But if this was the case then the outlet temperature is expected to be higher for the actual data than the design data and this is not the case, in the experimental data.

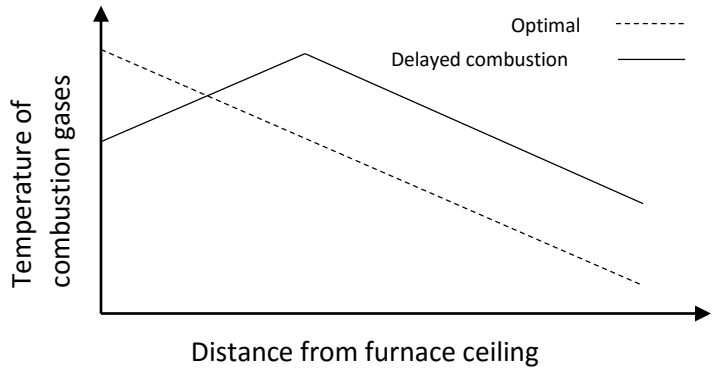

Figure 19. Delayed combustion.

The second possible explanation to the higher flow rate of fuel and air is that the heat transfer resistance has increased, e.g. due to fouling. This is illustrated in Figure 20. In this case the combustion is optimal, i.e. the initial temperature is at its maximum, but the lowered heat transfer rate has to be compensated by a higher flow rate. However, a higher outlet temperature is expected here as well and this is, once again, not the case.

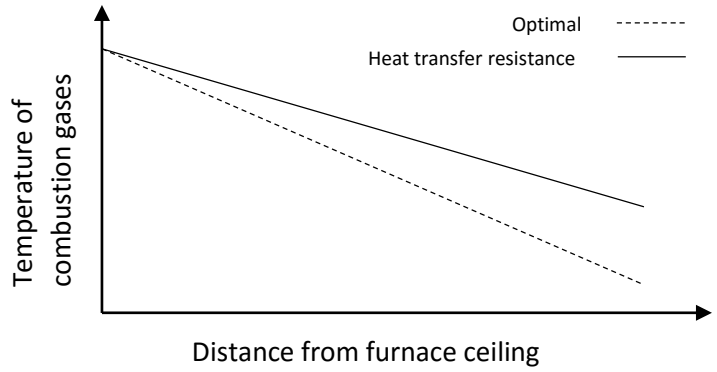

Figure 20. Increased heat transfer resistance.

The third possibility is that heat is lost to the atmosphere somewhere in the furnace, illustrated in Figure 21. In this case the outlet temperature could be the same, but the losses are compensated for by a higher flow rate. Such a leakage has however not been identified so far.

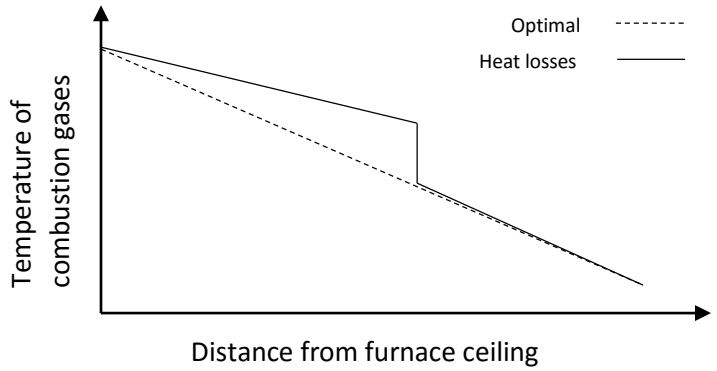

Figure 21. Heat is lost to the atmosphere.

According to the energy balance in Figure 8, the losses per amount of fuel is $3.6\ \%$ for the design conditions and $9.3\ \%$ for actual conditions. If the assumption is made that the actual losses are also $3.6\ \%$, i.e. $6.67\ MW$ instead of $17.3\ MW$. Then the heat of the flue gases leaving to convective section would increase to $103.6\ MW$ instead of $93.0\ MW$. Calculating the outlet temperature based on this assumption gives a value of $1375.59\ K$ instead of the temperature measured which is $1276.43\ K$. So, if the thermocouple measures a temperature that is around $100\ K$ lower than reality the first two reasons (delayed combustion or higher heat transfer resistance) are still possible explanations to the higher fuel consumption. The thermocouple is however valid for the temperature range and also shielded from radiation so there is nothing that implies that the measurement should be incorrect.

If the temperature measurement is correct and if the furnace is properly insulated there is no other explanation to the higher fuel consumption for the actual data except that the design data must have been too optimistic in the first place.

6 Conclusions

The energy balance showed that despite of the fact that production capacity between the design data and the actual data was almost exactly the same the actual data used approximately $10\ \%$ more heat as fuel for the combustion. Higher energy losses in the radiant section was identified as well as an increased amount of heat recovered in the convective section. The possible energy efficiency improvements based on the design data can thereby be found both in the radiant section and in the convective section.

The adiabatic flame temperature was calculated to $2104.8\ K$ for the design data and $2105.5\ K$ for the actual data. Since these temperatures are very similar it was concluded that the fuel consumption had not been increased to raise the flame temperature.

The composition of the fuel was varied by decreasing the amount of natural gas and the amount of tail gas in different ways, based on the idea to compensate a lower heating value with a raise of the flame temperature and thus possibly increase the heat transfer rate. It was possible to achieve a minor increase of the flame temperature, but the amount of energy needed in the convective section according to the design and actual data was unfortunately not sufficient. Additionally, it is not recommended to increase the flame temperature without more understanding of how it would affect the tube material, which already are under a very high stress at normal operational temperatures.

The CFD simulations that compared the design data and the actual data with respect to the mixing of fuel and air showed a very similar combustion process for the two cases. An improved mixing for the actual data was observed. This lead to higher temperatures in the upper part of the furnace. The temperature difference was small however; and it is difficult to tell if it could have a significant impact on the heat transfer. Especially since premixing and heat transfer were neglected in the simulations.

The main difference between the actual data and the design data are the higher flow rate of fuel and air. Unburnt fuel leaving the furnace could be excluded based on a gas chromatography analysis. A non-optimal mixing or a decreased heat transfer efficiency could explain why the flow rate has increased, but these two explanations do not agree with the temperature measurement of the flue gases at the outlet of radiant section. If this temperature is correctly measured the only remaining explanations to the higher fuel consumption is either higher losses of heat to the atmosphere somewhere in the radiant section or that the design data was too optimistically specified in the first place.

7 Further investigations

The conclusions from this project do not mean that it is not possible to improve the heat efficiency of the primary reformer. Some ideas that could lead to either better heat efficiency or at least more understanding are suggested here:

-Investigate the upper part of the burner, where the premixing occurs. CFD would be a suitable method for this. The physics are a bit challenging due to high velocities but the geometry is small. A good premixing most certainly optimizes the combustion.

-Analyze the energy demands in the convective section. Since the combustion in the radiant section affects the convective section it is important to have a proper understanding of what will happen in the heat recovery section before major changes are made. Additionally, a backward calculation from the flue gases leaving the stack could verify the temperature measurement at the outlet of radiant section.

-Investigate possibilities of using the tail gas as process gas instead of as fuel. The tail gas has a high amount of N_2, H_2 and CH_4. This makes it a suitable candidate.

-The CFD model could be further developed by including more phenomena, especially the premixing of the fuel, heat transfer to the tubes and radiation.

-The geometry could be increased in size if the computational capacity allows it. In that case it would be interesting to include the effect of the hot furnace walls on the heat transfer and the flow.

References

[1] Smil V. *Enriching the earth: Fritz Haber, Carl Bosch and the transformation of world food production*. Massachutes: The MIT press. 2001

[2] Organization for economic cooperation and development. *Indonesia policy brief: Agriculture* [Internet]. OECD. 2015. [cited 2015 Dec 20]. Available from: http://www.oecd.org/policy-briefs/indonesia-agriculture-improving-food-security.pdf

[3] Oberman R, Dobbs R, Budiman A, Thompson F, Rossé M. *The archipelago economy: Unleashing Indonesia's potential* [Internet]. McKinsey&Company. 2012. [cited 2015 Dec 20]. Available from: http://www.mckinsey.com/insights/asia-pacific/the_archipelago_economy

[4] Worrell E, Bernstein L, Roy J, Price L, Harnisch J. *Industrial energy efficiency and climate change mitigation*. Energy Efficiency. 2009;2(2):109-23

[5] Organization for economic cooperation and development. *OECD Review of agricultural policies: Indonesia 2012* [Internet]. OECD policies. 2012. [cited 2015 dec 20]. Available from: http://dx.doi.org/10.1787/9789264179011-en

[6] International fertilizer industry association. *About fertilizers* [Internet]. IFA. [cited 2015 dec 20]. Available from: http://www.fertilizer.org/AboutFertilizers

[7] Chaubey R, Sahu S, James OO, Maity S. *A review on development of industrial processes and emerging techniques for production of hydrogen from renewable and sustainable sources*. Renewable and Sustainable Energy Reviews. 2013;23:443

[8] Ebrahimi H, Behroozsarand A, Zamaniyan A. *Arrangement of primary and secondary reformers for synthesis gas production*. Chemical Engineering Research and Design. 2010;88(10):1342-50

[9] Dybkjaer I. *Tubular reforming and autothermal reforming of natural gas — an overview of available processes*. Fuel Processing Technology. 1995;42(2):85-107

[10] Xu J, Froment GF. *Methane steam reforming, methanation and water-gas shift: I. Intrinsic kinetics*. AIChE Journal. 1989;35(1):88-96

[11] Xu J, Froment GF. *Methane steam reforming: II. Diffusional limitations and reactor simulation*. AIChE Journal. 1989;35(1):97-103

[12] Farhadi F, Bahrami Babaheidari M, Motamed Hashemi MMY. *Radiative models for the furnace side of a bottom-fired reformer. Applied Thermal Engineering*. 2005;25(14):2398-411

[13] Grevskott S, Rusten T, Hillestad M, Edwin E, Olsvik O. *Modelling and simulation of a steam reforming tube with furnace*. Chemical Engineering Science. 2001;56(2):597-603

[14] Ramana Rao MV, Plehiers PM, Froment GF. *The coupled simulation of heat transfer and reaction in a pyrolysis furnace*. Chemical Engineering Science. 1988;43(6):1223-9

[15] Sanaye S, Baheri E. *Thermal modeling of radiation and convection sections of primary reformer of ammonia plant*. Applied Thermal Engineering. 2007;27(2):627-36

[16] Yu Z, Cao E, Wang Y, Zhou Z, Dai Z. *Simulation of natural gas steam reforming furnace*. Fuel Processing Technology. 2006;87(8):695-704

[17] Zamaniyan A, Ebrahimi H, Mohammadzadeh JSS. *A unified model for top fired methane steam reformers using three-dimensional zonal analysis*. Chemical Engineering & Processing: Process Intensification. 2008;47(5):946-56

[18] Sehested J, Gelten JAP, Remediakis IN, Bengaard H, Nørskov JK. *Sintering of nickel steam-reforming catalysts: effects of temperature and steam and hydrogen pressures*. Journal of Catalysis. 2004;223(2):432-43

[19] Rostrup-Nielsen J, Trimm DL. *Mechanisms of carbon formation on nickel-containing catalysts*. Journal of Catalysis. 1977;48(1):155-65

[20] Trimm DL. *Coke formation and minimization during steam reforming reactions*. Catalysis Today. 1997;37(3):233-8

[21] De Wilde J, Froment GF. *Computational Fluid Dynamics in chemical reactor analysis and design: Application to the ZoneFlow™ reactor for methane steam reforming*. Fuel. 2012;100:48

[22] Andersson B, Andersson R, Håkansson L, Mortensen M, Sudiyo R, van Wachem, B. G. M. *Computational Fluid Dynamics for Engineers*. Cambridge: Cambridge University Press; 2014

[23] Bailly C, Comte-Bellot G. *Turbulence*. Springer International Publishing; 2015

[24] United States National Aeronautics and Space Administration. *A new k-[epsilon] eddy viscosity model for high Reynolds number turbulent flows: model development and validation*. 1994

[25] Warnatz J. *The structure of laminar alkane-, alkene-, and acetylene flames*. Symposium (International) on Combustion. 1981;18(1):369-84

[26] Glassman I, Yetter RA, Glumac N. *Combustion*. 5 ed. Waltham, MA: Academic Press; 2015

[27] Warnatz J, Maas U, Dibble RW. *Combustion: physical and chemical fundamentals, modeling and simulation, experiments, pollutant formation*. 4 ed. Berlin: Springer; 2006

[28] Ansys Inc. *Ansys Fluent theory guide: release 15.0*. 2013

[29] National Institute of Standards and technology. *NIST Chemistry WebBook* [Internet]. NIST. 2015. [Cited 2015 dec 20]. Available from: http://webbook.nist.gov/chemistry

Appendix A – The fuel streams and their compositions

In Figure 22 the schematic for the different fuel streams to the primary reformer is visualized. The main fuel is natural gas, which also is used as fuel in the auxiliary boiler. Recycled tail gas and heavy hydrocarbon gas is also added to the primary reformer fuel.

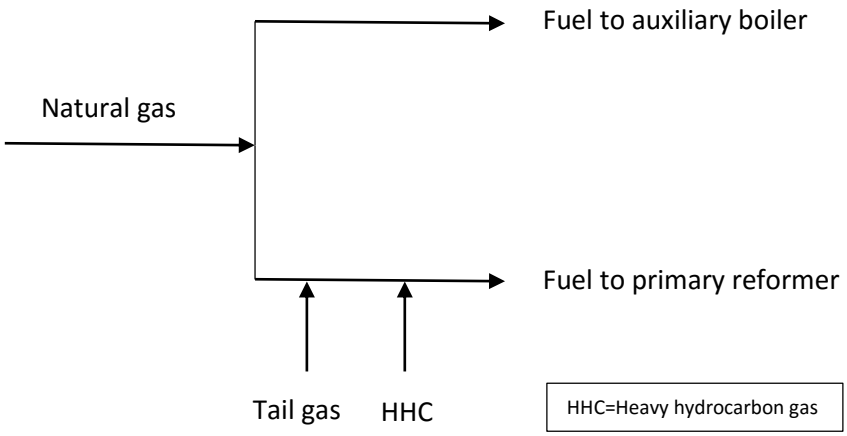

Figure 22. Fuel streams to primary reformer.

The compositions of the three fuel streams are presented in Table 5. The observant reader might notice that the compositions do not add up to exactly 100 %. The reason for this is merely due to a minor round-off error.

Table 5. Compositions of the different fuel streams to the primary reformer.

	Natural gas [%]	**Tail gas [%]**	**HHC [%]**
CH_4	84.1	13.0	3.4
C_2H_6	5.8	-	1.2
C_3H_8	1.5	-	33.7
i-C_4H_{10}	0.5	-	12.5
n-C_4H_{10}	0.4	-	18.1
i-C_5H_{12}	0.1	-	9.0
n-C_5H_{12}	0.1	-	5.9
C_6H_{12}	0.2	-	5.3
C_7H_{16}	-	-	5.7
CO_2	6.6	-	0.9
N_2	0.8	47.3	4.4
Ar	-	4.3	-
H_2	-	35.3	-
Flow rate [$kmol/h$]	537.7	345.4	63.7

Appendix B – Inlet compositions for actual and design simulations

Table 6. Inlet compositions, in mol fractions, for actual and design data used in the simulations.

	Actual		Design	
	Fuel inlet	**Air inlet**	**Fuel inlet**	**Air inlet**
CH_4	0.5274	-	0.6105	-
C_2H_6	0.0335	-	0.0425	-
C_3H_8	0.0312	-	0.0391	-
C_4H_{10}	0.0312	-	0.0288	-
C_5H_{12}	0.0257	-	-	-
C_6H_{14}	0.0044	-	-	-
C_7H_{16}	0.0039	-	-	-
H_2	0.1289	-	0.0546	-
NH_3	-	-	0.0033	-
N_2	0.1801	0.7748	0.1203	0.7748
O_2	-	0.2079	-	0.2079
H_2O	-	0.0078	-	0.0078
CO_2	0.0382	0.0003	0.0722	0.0003
Ar	0.0157	0.0092	0.0287	0.0092

Appendix C – Calculation of fuel consumption

The amount of unreacted fuel downstream from the fuel inlet was calculated according to Eq. (36)

$$Unreacted\ fuel = \int \frac{v_z x_b \rho + |v_z| x_b \rho}{2} dA \tag{36}$$

Where v_z is the velocity in the downward direction, x_b is the mass fraction of the fuel and ρ is the fluid density.

This equation ensures that any recirculation of fuel does not affect the net fuel consumption. Dividing by the total amount of fuel that enters at the fuel inlet gives the percentage of unburnt fuel.